TECHNICAL REPORT

ADS-15

THEORETICAL DETERMINATION OF CRASH LOADS FOR A LOCKHEED 1649 AIRCRAFT IN A CRASH TEST PROGRAM

Project No. 312-001-01H

July, 1964

FEDERAL AVIATION AGENCY

DISCLAIMER NOTICE

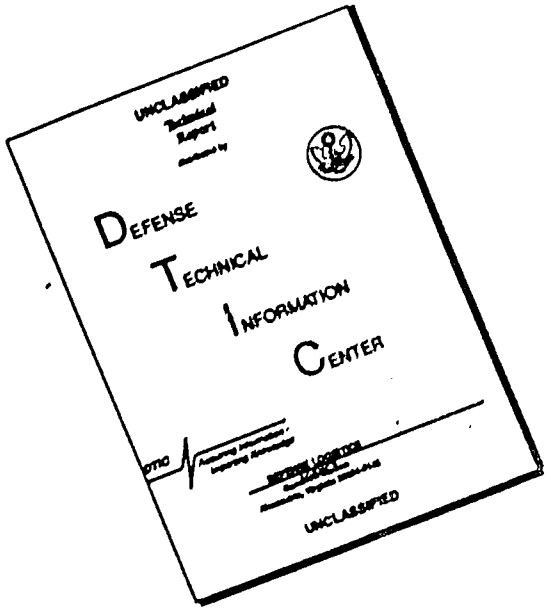

THIS DOCUMENT IS BEST QUALITY AVAILABLE. THE COPY FURNISHED TO DTIC CONTAINED A SIGNIFICANT NUMBER OF PAGES WHICH DO NOT REPRODUCE LEGIBLY.

BLANK PAGES
IN THIS
DOCUMENT
WERE NOT
FILMED

THEORETICAL DETERMINATION OF CRASH LOADS FOR A LOCKHEED 1649 AIRCRAFT IN A CRASH TEST PROGRAM

TECHNICAL REPORT

ADS-15

July, 1964

This report has been prepared by The Boeing Company, Airplane Division, for the Systems Research and Development Service, Federal Aviation Agency, under Contract No. FA64WA-5021. The contents of this report reflect the views of The Boeing Company, which is responsible for the facts and the accuracy of the data presented herein, and do not necessarily reflect the official views or policy of the FAA.

Prepared for

Federal Aviation Agency

Systems Research and Development Service

by

The Boeing Company

Airplane Division; Renton, Washington

THE BOEING COMPANY, Airplane Division
Renton, Washington
THEORETICAL DETERMINATION OF CRASH LOADS FOR A LOCKHEED 1649 AIRCRAFT IN A CRASH TEST PROGRAM; James P. Bigham, Jr. and William W. Bingham; July 1964
51 pages, 24 illustrations and 15 references for Type III Report
(FA64WA-5021)

ABSTRACT

Results of an analytical study to theoretically predict the loads to be experienced by a Lockheed Model 1649 Super Constellation during a controlled crash are presented. Acceleration time histories in directions normal and parallel to the fuselage cabin floor are given at three positions along the length of the fuselage for impact velocities of 140, 160, 180, and 200 feet per second. Results of investigations of the effects of variations in important problem parameters are also presented.

It is concluded that during the initial impact at 180 feet per second, peak normal accelerations of 11, 0, and -3 times that of gravity (G's) will be developed 0.03 seconds after impact at Body Stations 180, 682, and 1176. Maximum normal and longitudinal accelerations during the 6 degree ramp crash will occur at 0.24 seconds. Maximum normal accelerations at Body Stations 180, 682, and 1176 will be -17, 8, and 35 G's respectively. Maximum longitudinal accelerations will be 4 G's.

It is further concluded that the nose of the airplane will bend upwards 10 inches relative to the center section of the fuselage 0.14 seconds after impact. This deflection will probably be of sufficient magnitude to exceed the ultimate strength of the fuselage above the cabin floor. If the fuselage should fail, all analytical results beyond the time of failure will be questionable to a degree dependent on the type of failure that occurs.

INITIAL CONDITIONS – FLEXIBLE BODY			
SPEED	180 FT./SEC.	C.G. LOCATION–BODY STA.	682
ANGLE OF IMPACT	6 DEGREES	PLOWING COEFFICIENT	80 LB./IN.^{2}
WEIGHT	124,500 LBS.	PLOWING AREA	700 IN.^{2}
INERTIA ABOUT C.G.	4.64×10^9 LB./IN.^{2}	FRICTION COEFFICIENT	.3

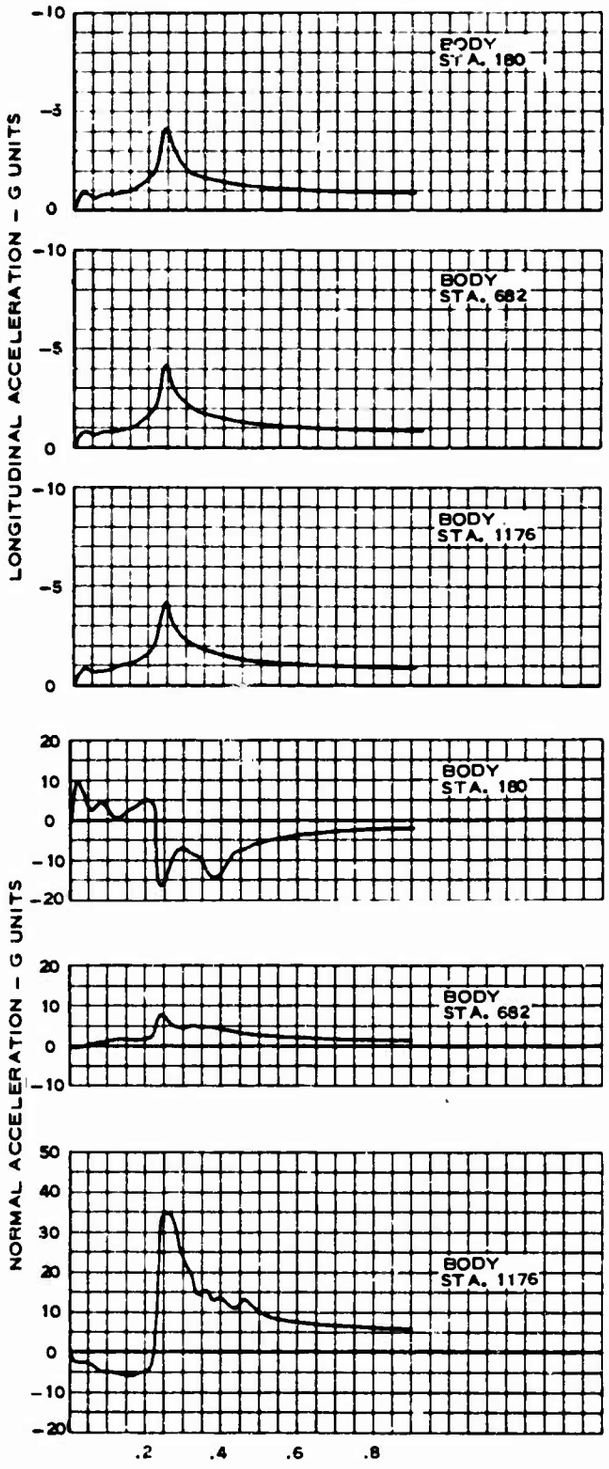

TABLE OF CONTENTS

LIST OF ILLUSTRATIONS

LIST OF SYMBOLS

A	Effective cross sectional area of fuselage - $in.^2$
A_p	Fuselage plowing area - $in.^2$
c	Linear damping coefficient - lb/in. /sec
C_p	Plowing coefficient - $lb/in.^2$
E	Effective bulk modulus of elasticity of fuselage - $lb/in.^2$
$F(t)$	Longitudinal forcing function at nose of airplane - lb
F_D	Damping force - lb
F_f	Friction force - lb
F_N	Force normal to ramp surface - lb
F_p	Plowing force - lb
F_q	Total generalized force acting in body vertical bending degree of freedom - lb
F_{sp}	Spring force - lb
F_x	Total force acting in x direction - lb
F_y	Total force acting in y direction - lb
g	Structural damping coefficient - dimensionless
G	Acceleration due to gravity - 386 $in./sec^2$
h	Distance from airplane center of gravity to any point on the airplane measured perpendicular to the body centerline - + down - in.
I	Total airplane pitching moment of inertia about its center of gravity - lb in. sec^2
I_k	Pitching moment of inertia of kth mass - lb in. sec^2
K_g	Equivalent linear spring stiffness of the ground spring - lb/in.
K_s	Spring stiffness of fuselage understructure - lb/in.
K_1	Defined in Fig. 5 - lb/in.
K_2	Defined in Fig. 5 - lb/in.

ℓ	Distance from airplane center of gravity to any point on the airplane measured parallel to the body centerline - + forward - in.
L	Total effective length of fuselage - in.
m_k	Mass of kth point - lb sec^2/in.
M	Total mass of airplane - lb sec^2/in.
n	Total number of springs representing the fuselage understructure
nn	Total number of lumped masses representing the airplane
q	Displacement in the fuselage vertical bending mode at the nose of the airplane - + down - in.
Q	Generalized force in the Lagrangean equation
r	Combined transmissibility and structural damping factor in fuselage longitudinal vibrations - dimensionless
R_x	Moment arm of F_x about the airplane center of gravity - in.
R_y	Moment arm of F_y about the airplane center of gravity - in.
s	Speed of sound in fuselage structure - in./sec
t	Time - seconds
t_A	Defined by Equation (36)
t_B	Defined by Equation (37)
t_o	Defined by Equation (33)
t_1	Defined by Equation (34)
T	Kinetic energy - in. lb
u	Displacement of fuselage in longitudinal vibration - in.
U	Potential energy - in. lb
v	Displacement of airplane perpendicular to ramp surface - in.
x	Horizontal rigid body displacement of airplane center of gravity - in.
$\bar{x}$	Displacement parallel to cabin floor measured from nose of aircraft - in.
$\ddot{\bar{x}}$	Acceleration parallel to cabin floor - in./sec^2

y	Vertical rigid body displacement of airplane center of gravity - in.
$\ddot{y}$	Acceleration perpendicular to cabin floor - in./sec^2
α	Pitch about the airplane center of gravity - rad
β	Defined by Equation (38)
δ_g	Deflection of ground spring - in.
δ_s	Deflection of structural spring - in.
δ_1	Defined in Fig. 5
δ_2	Defined in Fig. 5
$\Delta\bar{x}$	Change in length of fuselage - in.
Θ	Ramp angle - rad
λ	Defined by Equation (39)
μ	Friction Coefficient - Dimensionless
M_α	Total moment acting in α rotation - in. lb
Ξ	Generalized mass - lb sec^2/in.
ρ	Density of fuselage structure - lb sec^2/in.^{4}
σ_x	Fuselage longitudinal unit stress - lb/in.^{2}
τ	Period of longitudinal fuselage vibration - sec
ϕ	Normalized deflection of fuselage bending mode - dimensionless
ϕ'	Normalized slope of fuselage bending mode - rad/in.
ψ_1	Defined in Fig. 5
ψ_2	Defined in Fig. 5
ω	Frequency of fuselage bending mode - rad/sec

The dot notation is used to indicate differentiation with respect to time. For example:

$$\dot{x} = \frac{dx}{dt} \qquad \ddot{x} = \frac{d^2x}{dt^2}$$

1.0 INTRODUCTION

This report presents the results of an analytical study to theoretically determine the loads to be experienced by a Lockheed Model 1649 Super Constellation during a controlled crash. A specific requirement of this study was the calculation of acceleration time histories in directions parallel and normal to the cabin floor at Fuselage Stations 180, 682, and 1176. This was done for each of four initial impact velocities: 140, 160, 180, and 200 feet per second. Data of this type can be used to calculate the forces that would be experienced during the crash by passengers, crew, or cargo located in the airplane.

The determination of the loads in an aircraft during a marginally survivable crash is a complex problem and depends upon many factors. Among the more important of these factors are the initial velocity of the airplane, its attitude relative to the ground and to its flight path, its geometry and weight, the type of surface on which it impacts, and the deformation characteristics of its structure. If an analytical method could be found to define, with a reasonable degree of accuracy, marginally survivable crash loads for different types of aircraft, information obtained would be invaluable in the development of equipment for the safety of passengers and crew. Included in this equipment would be such items as airplane structure, passenger seats, safety harnesses, shock absorption systems, and cargo restraint systems. The study reported in this document represents an attempt to develop such an analytical method.

The airplane of this analysis is a Lockheed Model 1649 Super Constellation (Fig. 3). Its configuration is identical to that to be used by the Federal Aviation Agency in an actual crash test of the Lockheed 1649 currently scheduled for August 1964. The specific conditions of this test are as follows (Ref. 2):

- The airplane is to impact nose first into a 6 degree dirt ramp at a velocity of approximately 180 feet per second.
- At impact, the longitudinal axis of the fuselage is to be horizontal to the ground at the base of the ramp and the wings are to be level.
- The yaw angle of the airplane relative to its flight path is zero.
- The wing lift is completely destroyed.
- The landing gear and wings outboard of Wing Station 484 are to have completely separated from the airplane.

These initial test conditions are considered to be of a marginally survivable nature, and simulate a crash condition such as might be experienced in an aborted takeoff.

It is to be emphasized that the results of this report apply only to the airplane as it passes over the 6 degree ramp. At a distance of approximately 200 feet from the initial impact point the ramp slope increases sharply. At this point these results are no longer valid. It is also be emphasized that this analysis assumes the portion of the airplane above the cabin floor remains

intact during the 6 degree ramp crash. If this part of the fuselage should fail at any time during the crash, the analytical results beyond that time would be questionable. How much the accuracy of the results would be affected would depend largely on the type of failure that occurred. For example, if the fuselage forward of the leading edge of the wing separated from the airplane, the physical characteristics of the airplane would change substantially, and analytical data for times after this failure would not be reliable. This is covered in additional detail in Section 4.2.1.

The discussion of this report is divided into five sections. The first section explains the basic equations used in the analysis. These equations are derived in three steps. The airplane is first treated as a rigid body free to pitch and to translate horizontally and vertically in space. Next, the vertical bending flexibility of the fuselage is included, and, finally, equations for the longitudinal vibration of the fuselage are obtained. Also included in the first section is a brief discussion of the digital program used for the solution of the mathematical equations.

The second section of this report discusses the computation of the basic problem input data. The third section presents the major results. In the first part of this section, acceleration time histories are given for both the rigid body analyses and for those in which the vertical bending and longitudinal flexibilities of the fuselage are considered. Because of the large number of variables involved in the analyses and the difficulties of mathematically representing or experimentally determing these variables, a parametric study is described in the second part of the third section.

The important conclusions of this theoretical study and recommendations for future work are given in the final sections of this report.

As mentioned previously, the calculation of crash loads is complex and necessarily involves many approximations. For this reason, if the correct trends of the acceleration time histories are predicted, and if the peak acceleration values and times at which they occur do not deviate more than 25 percent from the experimental data, it is believed good agreement between analytical and experimental results will have been realized. As experience is gained, it is expected that the accuracy of the analysis could be improved.

2.0 BASIC THEORY

This section describes the mathematical equations used to determine the motion of the airplane during the crash. It is divided into three main subsections. The first subsection discusses the rigid body equations; that is, those equations in which the vertical bending and longitudinal flexibilities of the airplane are not considered. The second gives those equations which account for the effects of airplane vertical bending and longitudinal vibrations. The third subsection briefly describes the technique used in the solution of the mathematical equations.

2.1 THE RIGID BODY EQUATIONS

2.1.1 Assumptions

In the derivation of the rigid body equations, the following assumptions were made:

- The crash is symmetric. That is, the airplane is free to pitch and translate vertically and horizontally during and after initial impact, but cannot roll, yaw, or translate laterally.
- At initial impact the wings are level to the surface of the ramp and the yaw angle of the airplane relative to its forward motion is zero.
- The wing lift is completely destroyed.
- The bottom of the fuselage is made up of a finite number of nonrestoring, nonlinear springs in parallel with nonreversible linear dampers.

2.1.2 The Equations

The following are the equations used to describe the rigid body motion. A drawing of the coordinate system is shown in Fig. 1, and the definitions of symbols are given in the list of symbols.

The x-y coordinates of the ith point on the airplane are:

$$x_i = x + \ell_i \cos\alpha + h_i \sin\alpha \tag{1}$$

$$y_i = y - \ell_i \sin\alpha + h_i \cos\alpha \tag{2}$$

The normal distance from the ith point on the airplane to the ramp is therefore:

$$v_i = x_i \sin\theta_i + y_i \cos\theta_i \tag{3}$$

Note that the ramp can have two angles (Fig. 1) with the change in ramp slope occurring at the origin of the coordinate system. Note also that according to the chosen sign convention the ith point is in contact with the ramp only if v_i is

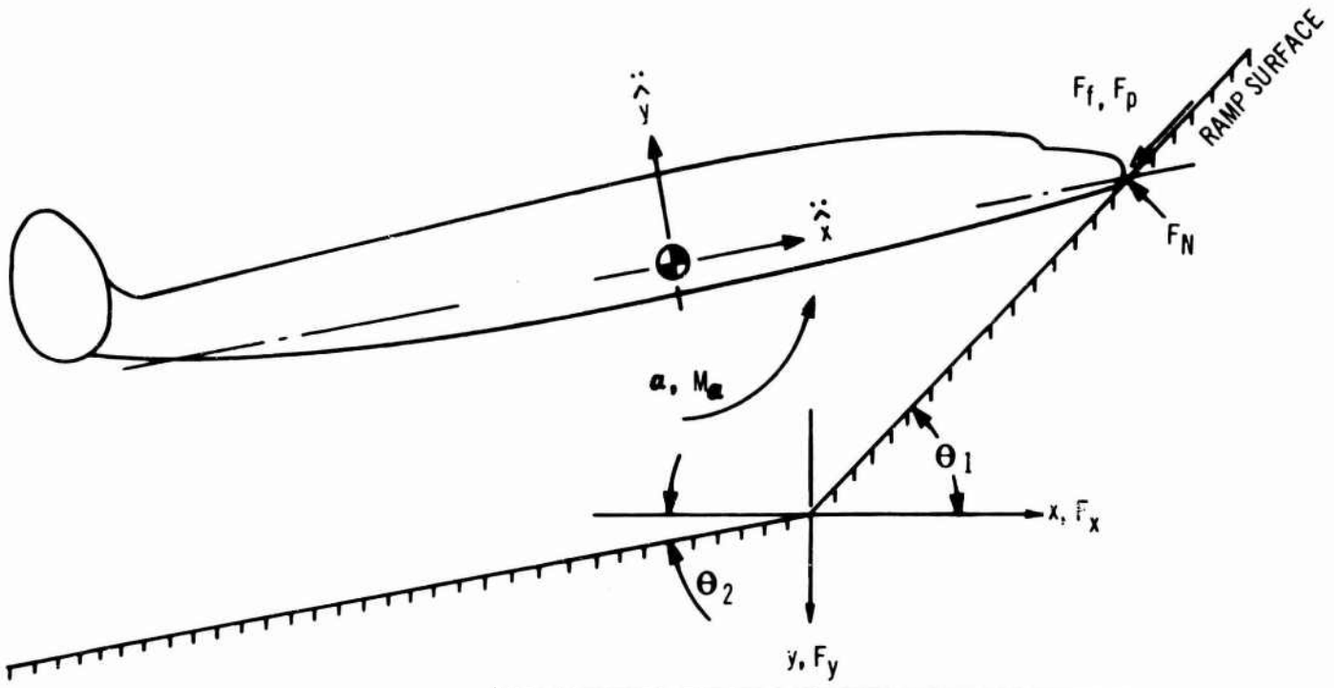

FIG. 1 SIGN CONVENTION USED IN DERIVATION OF EQUATIONS

greater than zero. v_i, then, can be used directly to determine the deflection and, therefore, the force in the nonrestoring springs and dampers representing the bottom of the fuselage.

Each structural spring along the base of the fuselage is assumed to be in series with a spring representing the ground. The total deflection of these two springs at the ith station must then equal v_i for values of v_i greater than zero.

$$v_i = \delta_{s_i} + \delta_{g_i} \tag{4}$$

Because the springs are in series the force in each of these springs must be equal at all times.

$$\delta_{s_i} K_{s_i} = \delta_{g_i} K_{g_i} = F_{sp_i} \tag{5}$$

A viscous damper to represent the combined damping characteristics of the ground and structure can be placed in parallel with each ith spring. Again, for values of v_i greater than zero, the damping force is then:

$$F_{D_i} = \dot{v}_i c_i \tag{6}$$

The force acting on the airplane normal to the ground surface at the ith location is:

$$F_{N_i} = F_{sp_i} + F_{D_i} \tag{7}$$

The total forces acting on the airplane parallel to the ground surface are considered to consist of friction and plowing forces. The friction force at the ith station is:

$$F_{f_i} = \mu F_{N_i} \tag{8}$$

The plowing force is assumed to be a constant force acting at any time the airplane is in contact with the ramp. This is not correctly true since the plowing area of the airplane is related to the deformation of the ground and to the airplane understructure. However, because of the difficulties of analytically determining exact ground and airplane understructure deformation, it is believed the assumption of a constant plowing force is adequate. This is discussed in more detail in Section 4.3.5.

The plowing force is then:

$$F_p = A_p C_p \tag{9}$$

Calculating the components in the x and y directions of forces normal and parallel to the ramp:

$$F_x = -\sum_{i=1}^{n} \left[F_{N_i} \sin\theta_i + F_{f_i} \cos\theta_i \right] - F_p \cos\theta_1 \tag{10}$$

$$F_y = -\sum_{i=1}^{n} \left[F_{N_i} \cos\theta_i - F_{f_i} \sin\theta_i \right] + F_p \sin\theta_1 \tag{11}$$

Note that the ramp angle at the nose is used with the plowing force. The moment arms of F_{x_i} and F_{y_i} about the airplane center of gravity are:

$$R_{x_i} = h_i \cos\alpha - \ell_i \sin\alpha \tag{12}$$

$$R_{y_i} = h_i \sin\alpha + \ell_i \cos\alpha \tag{13}$$

And the total moment about the airplane center of gravity is:

$$M_\alpha = \sum_{i=1}^{n} \left[-R_{x_i} (F_{N_i} \sin\theta_i + F_{f_i} \cos\theta_i) + R_{y_i} (F_{N_i} \cos\theta_i - F_{f_i} \sin\theta_i) \right] - R_{x_1} F_p \cos\theta_1 - R_{y_1} F_p \sin\theta_1 \tag{14}$$

Setting F_x, F_y, and M_α equal to the inertia forces in the system gives:

$$M\ddot{x} = F_x \tag{15}$$

$$M\ddot{y} = F_y + MG \tag{16}$$

$$I\ddot{\alpha} = M_\alpha \tag{17}$$

Using the above equations to determine $\ddot{x}$, $\ddot{y}$, and $\ddot{\alpha}$, the relative accelerations parallel and normal to the fuselage floor at the jth point can be calculated:

$$\ddot{\hat{x}}_j = \ddot{x}\cos\alpha - \ddot{y}\sin\alpha - \ell_j \dot{\alpha}^2 + h_j \ddot{\alpha} + G\sin\alpha \tag{18}$$

$$\ddot{\hat{y}}_j = -\ddot{x}\sin\alpha - \ddot{y}\cos\alpha + h_j \dot{\alpha}^2 + \ell_j \ddot{\alpha} + G\cos\alpha \tag{19}$$

The first two terms of each of the above equations are the components of the x and y accelerations acting parallel and normal to the fuselage floor. The third terms account for centrifugal force effects, and the fourth for accelerations caused by pitch of the airplane. The final terms remove the effect of gravity making the accelerations relative rather than absolute.

Equations (1) through (19), then, comprise the basic rigid body equations for the symmetrical crash of an airplane into a wedge-shaped ramp.

2.2 THE FLEXIBLE BODY EQUATIONS

In the derivation of the flexible body equations, the assumptions of Section 2.1.1 were used. As the crash was considered to be symmetric, the only airplane flexibilities considered were those in the vertical bending and longitudinal directions. These will be discussed individually.

2.2.1 Vertical Bending of the Fuselage

The displacement of the fuselage in its first vertical bending mode is represented by the single generalized coordinate "q." The displacement normal to the fuselage longitudinal axis of the ith point on the fuselage is then $\phi_i q$ where ϕ_i is the mode shape weighting function as given in Fig. 6.

Calculating the kinetic and potential energies of the airplane in its first vertical bending mode, and differentiating according to the Lagrangean equation

$$\frac{d}{dt}\left(\frac{\partial T}{\partial \dot{q}}\right) + \frac{\partial U}{\partial q} = Q \tag{20}$$

gives the equation of motion for the vertical bending degree of freedom

$$\Xi \ddot{q} = -\Xi \omega^2 q + F_q \tag{21}$$

where Ξ is the generalized mass of the fuselage in its first vertical bending mode and is defined by the equation

$$\Xi = \Sigma_{k=1}^{nn} \left[m_k \phi_k^2 + I_k \phi'^2_k \right] \tag{22}$$

The right side of Equation (21) consists of two terms. The first is the generalized stiffness of the vertical bending degree of freedom. The sec-

ond term is the generalized force and is determined by the equation

$$F_q = \sum_{i=1}^{n} \left[F_{N_i} \phi_i \cos(\theta_i - \alpha) + F_{f_i} \phi_i \sin(\theta_i - \alpha) \right] \tag{23}$$

$$+ F_p \phi_1 \sin(\theta_1 - \alpha)$$

v_i must now be redefined. Taking q as positive nose down

$$v_i = x_i \sin \theta_i + y_i \cos \theta_i + \cos(\theta_i - \alpha) - \phi_i q \tag{24}$$

The accelerations normal and parallel to the cabin floor at the jth point are:

$$\ddot{\hat{x}}_j = \ddot{x} \cos \alpha - \ddot{y} \sin \alpha - \ell_j \dot{\alpha}^2 + h_j \ddot{\alpha} + G \sin \alpha \tag{25}$$

$$\ddot{\hat{y}}_j = -\ddot{x} \sin \alpha - \ddot{y} \cos \alpha + h_j \dot{\alpha}^2 + \ell_j \ddot{\alpha} + G \cos \alpha - \phi_j \ddot{q} \tag{26}$$

With the exception of Equation (3), Equations (1) through (17) from Section 2.1.2 together with (21) through (26) above are the equations describing the symmetrical crash of an airplane having fuselage vertical bending flexibility.

2.2.2 Longitudinal Fuselage Vibrations

In addition to the assumptions of Section 2.1.1, the following assumptions were used in the derivation of the equations for fuselage longitudinal vibrations.

1. The fuselage is a continuous beam with constant weight, density, and bulk modulus of elasticity along its length.

2. The continuous beam representing the fuselage is in a fixed-free end condition. That is, the nose of the airplane is not free to displace longitudinally relative to its rigid body displacement.

3. The longitudinal vibrations are dependent only on the longitudinal accelerations experienced by the airplane during the crash and are not affected by forces or accelerations normal to the longitudinal axis of the fuselage.

4. The total longitudinal acceleration of the airplane is the sum of its rigid and flexible body accelerations.

These assumptions are severe, and were made to allow approximate answers to be obtained in a reasonable period of time. A more accurate mathematical representation could be derived, but the complexity of the equations would be formidable. Since results have shown that the effects of longitudinal vibrations of the fuselage are small relative to the rigid body accelerations, and would probably be even smaller if more exact mathematical equations were used, the theory of this report is believed to be adequate.

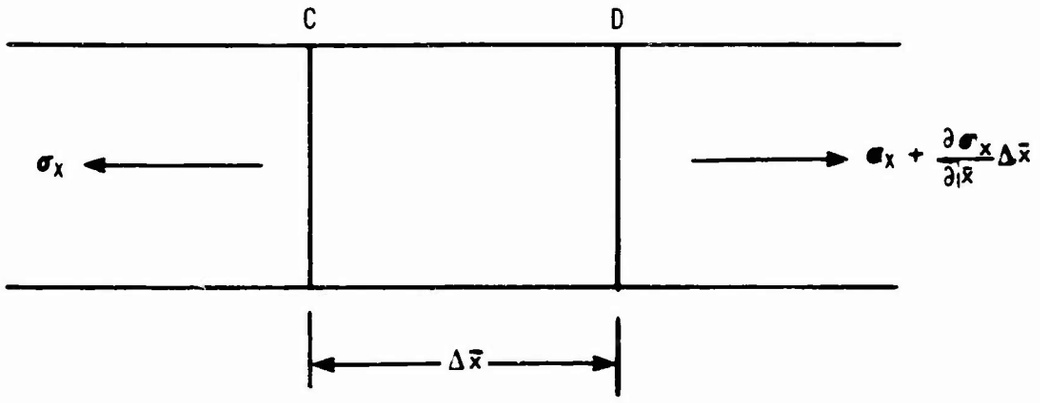

FIG. 2 FORCES ACTING ON ELEMENT OF BAR IN LONGITUDINAL MOTION

Assuming a beam of constant weight, density, and bulk modulus, the forces acting on an element of the beam can be written. Consider a small element CD of length $\Delta \bar{x}$ (Fig. 2) and let the cross-sectional area of the beam be A. The unit stress on the face through C is σ_x and the stress on the face through D is therefore $\sigma_x + (\partial \sigma_x / \partial \bar{x}) \Delta \bar{x}$. Letting the longitudinal displacement of the element be u, we have from Newton's second law of motion:

$$\rho A \Delta \bar{x} \frac{\partial^2 u}{\partial t^2} = A \frac{\partial \sigma_x}{\partial \bar{x}} \Delta \bar{x} \tag{27}$$

where the left side of the equation is the mass of the element times its acceleration and the right side is the force causing the acceleration. Canceling equal terms on either side of (27) and differentiating with respect to $\bar{x}$

$$\rho \frac{\partial \ddot{u}}{\partial \bar{x}} = \frac{\partial^2 \sigma_x}{\partial \bar{x}^2} \tag{28}$$

Making use of the relation

$$E \frac{\partial u}{\partial \bar{x}} = \sigma_x$$

and differentiating both sides twice with respect to time

$$E \frac{\partial \ddot{u}}{\partial \bar{x}} = \ddot{\sigma}_x \tag{29}$$

Note that in (29), $\bar{x}$ is considered not to be a function of time as specified by Assumption (4) at the beginning of this section. Substituting in (28)

$$\rho \ddot{\sigma}_x = E \frac{\partial^2 \sigma_x}{\partial x^2} \tag{30}$$

It has been shown that the speed of sound in a homogeneous bar is:

$$s = \sqrt{E/\rho} \tag{31}$$

Equation (30) then becomes:

$$\ddot{\sigma}_x = s^2 \frac{\partial^2 \sigma_x}{\partial \bar{x}^2} \tag{32}$$

The following are the boundary conditions:

$$\sigma_x(o, t) = \frac{F(t)}{A} \quad And \quad \sigma_x(L, t) = 0$$

where L is the $\bar{x}$ coordinate of the beam at its free end and F(t) is the longitudinal force caused by the rigid body motions.

Equation (32) can be solved by a numerical method. This is explained more completely in Ref. 3. The general procedure is to define the impact force function F(t) at the nose of the airplane ($\bar{x} = 0$). The initial stress F(t)/A is considered to travel along the bar as a compressive wave. Upon reaching the aft or free end of the fuselage it reflects back as a tensile stress wave. When this reflected wave reaches the nose or impact end of the fuselage it again reflects back through the fuselage as a compressive stress wave with reduced intensity. Looking at a particular point $\bar{x}_j$ along the length of the fuselage it initially takes time

$$t_o = \frac{\bar{x}_j}{s} \tag{33}$$

for the stress wave to reach points $\bar{x}_j$. It also takes time

$$t_1 = \frac{2L - \bar{x}_j}{s} \tag{34}$$

for the stress wave to reach point $\bar{x}_j$ after reflecting back from the free end $\bar{x} = L$. This process is repeated with period $\tau = 2L/s$, and the magnitude decreases each time by a factor r. The stress at $\bar{x}_j$, then, can be obtained by algebraically summing the original and reflected stress waves. The mathematical expression of the resultant stress can be written:

$$\sigma_x(\bar{x}_j, t) = \frac{1}{A} \sum_{m=0} \left\{ \beta r^m F(t-t_A) - \gamma F(t-t_B) \right\} \tag{35}$$

where:

$$t_A = t_o + m\tau \tag{36}$$

$$t_B = t_1 + m\tau \tag{37}$$

and β and γ are step functions such that:

$$\beta = 0 \quad For \; 0 \le t \le t_A$$

$$\beta = 1.0 \quad For \; t > t_A \tag{38}$$

$$\lambda = 0 \quad For \ 0 \leq t \leq t_B$$
$$\lambda = 1.0 \quad For \ t > t_B \tag{39}$$

The first term in (35) within the range of the summation sign represents the compressive waves, and the second term is the contribution to the total stress of the tensile waves.

Having obtained the stress function $\sigma_x(\bar{x}_j, t)$, the acceleration at station $\bar{x}_j$ can be calculated by differentiating σ_x with respect to $\bar{x}$ at the jth point and substituting in Equation (27).

$$\ddot{u}_j = \frac{1}{\rho} \left(\frac{\partial \sigma_x}{\partial \bar{x}} \right)_j \tag{40}$$

The total longitudinal acceleration at any point along the fuselage is then:

$$\ddot{\bar{x}}_j + \ddot{u}_j \tag{41}$$

by Assumption (4)

2.3 SOLUTION OF THE EQUATIONS

The differential equations of motion derived in Sections 2.1 and 2.2 are of second order and are nonlinear. For this reason, the technique of numerical integration was used to solve them. The solution program employed was the dynamic analyzer (DYANA) program described in Ref. 7. This program utilizes the Runge-Kutta method of numerical integration, a description of which can be found in Refs. 11 and 13. Essentially, in numerical integration, the acceleration, velocity, and displacement of the coordinates of the system are computed over a given time interval. These computed qualities are then used as initial conditions for the next time interval in the evaluation of acceleration, velocity, and displacement at the end of that time interval. Generally speaking, for a given time range decreasing the time interval of integration increases the accuracy of the answer. In the solution of the equations of Sections 2.1 and 2.2, a time range of 0.9 seconds was selected, and integrations were performed at intervals of 0.001 seconds within that range. Answers were printed at increments of 0.02 seconds.

3.0 BASIC INPUT DATA

This section discusses the calculation of the basic problem input data. A drawing of the Model 1649 is given in Fig. 3.

3.1 AIRPLANE WEIGHT AND INERTIA

The airplane weight properties were estimated from data supplied by both Lockheed and the Federal Aviation Agency. Fig. 4 shows the weight distribution used in the analysis. The separation from the airplane of the wings outboard of Wing Station 484 has been accounted for in this listing.

3.2 AIRPLANE STRUCTURAL STIFFNESS DATA

3.2.1 Flexibility of the Fuselage Understructure

During impact of the airplane into the ramp, energy is absorbed by the crushing of the understructure of the fuselage. It is important, then, that in a crash loads analysis that the crushing characteristics of the fuselage understructure be represented.

The bottom of the fuselage is, of course, a continuous structure. It was necessary for calculative purposes, however, to consider it as consisting of a finite number of springs in parallel along the length of the fuselage. A total of 20 were used, and a listing of their properties is given in Fig. 5. With reference to the sample stiffness-deflection curve shown at the top of Fig. 5, the springs were considered to be elastic (restoring) within the range of $_1$. When the deflection of the spring increased beyond $_1$, however, the structure was considered to be permanently deformed (plastic) and the spring was therefore not restoring. The downward slope of the stiffness curve between $_1$ and $_2$ represents the decrease in effective spring stiffness because of exceedence of the elastic limit. The upward slope of the curve beyond $_2$ accounts for the increase because of the stiffer structure of the cabin floor and wing.

Basic information on 1649 fuselage frame and bulkhead spacing and construction was furnished by Lockheed. This was used to determine the spring properties of Fig. 5. The general procedure was to divide the fuselage into sections of varying length based on geometry and location of bulkheads. The deflection per unit load of the frames and bulkheads within each section was then calculated using the methods of Ref. 12. This gave the stiffness of the section up to that deflection at which the frame or bulkhead yields due to elastic instability. This stiffness is shown as K_1 in the drawing of Fig. 5. The stiffness of the sections for deflections beyond the elastic limit was estimated. If the geometry of each section did not change as the understructure was crushed, it would be expected that once the elastic limit was exceeded, the crushing force would remain relatively constant as the deflection increased. However, since, as the understructure of the 1649 crushes, additional material picks up the load, it is believed the estimated stiffness values give a good approximation of the force-deflection characteristics of the structure.

In the calculation of this stiffness data, the contribution of the nacelles was not considered to be significant. This may not be strictly true as the oil

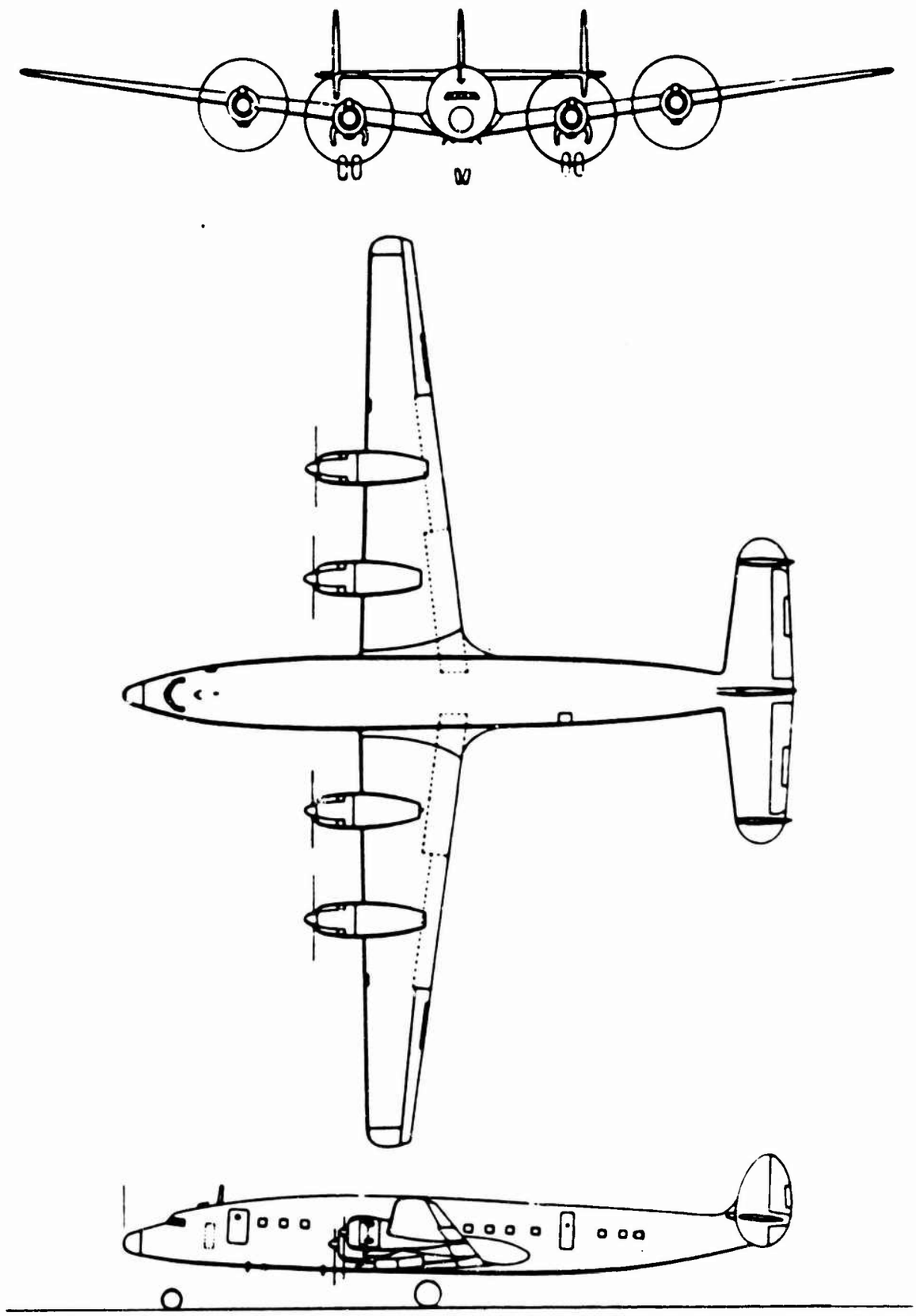

FIG. 3 THE LOCKHEED MODEL 1649 SUPER CONSTELLATION

cooler air intake ducts on the bottom of the inboard nacelles extend about one foot below the fuselage. It is believed, however, that the nacelle structure is relatively weak, and will be separated from the airplane when it contacts the propeller barriers prior to ramp impact (Ref. 2).

3.2.2 Body Flexibility

The vertical bending stiffness (EI) of the fuselage for the calculation of the fuselage vertical bending mode was furnished by Lockheed. A listing of this data is given in Fig. 4.

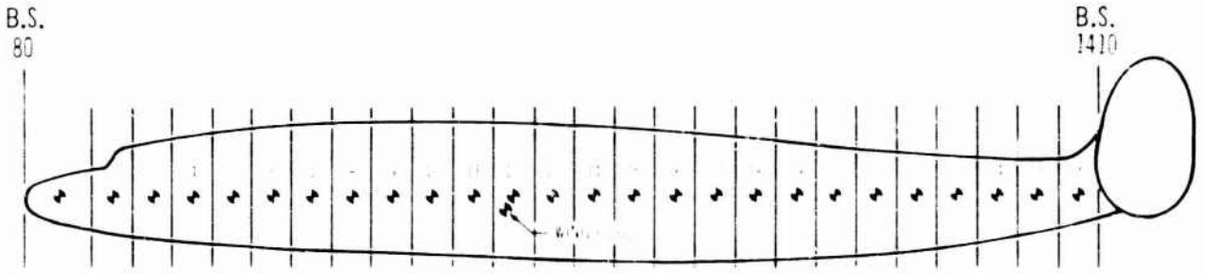

PANEL NO.	BODY STATION	WEIGHT LBS	E.I. x 10^{-10} LB IN^2
1	138.4	514	1.0
2	193.4	2471	3.0
3	239.5	2359	10.0
4	284.5	1872	17.5
5	334.0	1844	25.0
6	384.6	1809	33.0
7	435.6	1723	38.0
8	483.7	4815	39.5
9	534.4	4805	47.0
10	584.7	1897	58.5
11	636.7	2903	75.0
W.C.	648.0	75748	RIGID
12	681.7	2263	RIGID
13	731.4	1940	RIGID

PANEL NO.	BODY STATION	WEIGHT LBS	E.I. x 10^{-10} LB IN^2
14	783.1	2331	80.0
15	836.8	1862	79.0
16	884.1	1682	63.0
17	933.0	1656	58.0
18	984.1	1685	54.0
19	1034.6	1579	40.0
20	1083.5	1542	33.0
21	1130.4	503	26.0
22	1182.9	377	18.0
23	1237.1	343	12.5
24	1269.8	233	10.0
25	1330.9	255	7.5
26	1391.9	3264	5.0
27	1428.3	225	1.0
TOTAL	682.0	124 500	

FIG. 4 BASIC WEIGHT AND STIFFNESS DATA – THE LOCKHEED MODEL 1649

3.3 FUSELAGE VERTICAL BENDING MODE

To obtain the frequency and mode shape of the fuselage first vertical bending mode, the fuselage was divided into three principal sections: that section of the fuselage forward of and cantilevered from the wing front spar, the fusealge aft of and cantilevered from the wing rear spar, and the section of the fuselage between the wing spars. The fore and aft fuselage sections were considered to be flexible while the center body was treated as a rigid member. The first cantilevered vertical bending mode of the fore and aft fuselage were

determined using the influence coefficient method described in Chapter 4 of Ref. 14. These vertical bending modes of the fore and aft bodies were then coupled with rigid body pitch and vertical translation by means of Lagrange's Equation (20). The Rayleigh-Ritz method also described in Ref. 14 was then used to compute the first unrestrained vertical bending mode of the fuselage. The normalized mode shape is given in Fig. 6.

3.4 OTHER DATA

Information on the calculation of other parameters such as fuselage plowing area, friction coefficient, ground stiffness, etc., is contained in Section 4.3.

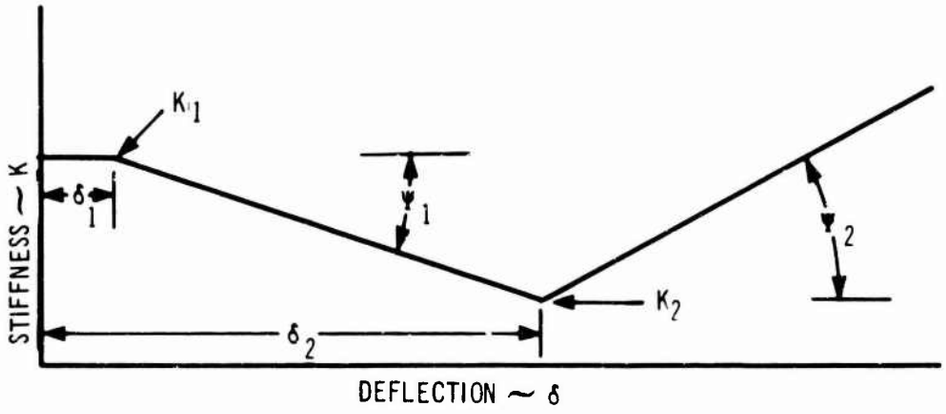

	BODY STA.	FUSELAGE SECTION LENGTH	FUSELAGE DIAMETER	SPRING LOCATION	K_1	K_2	δ_1	δ_2	TANGENT Ψ_1	TANGENT Ψ_2
		INCHES	INCHES	B.S.	LB./IN.		IN.	IN.	LB./IN./IN.	
1	80– 180	100	54	130	12000	5000	2	8	-1165	1165
2	180– 260	80	100	230	9600	4000	3	20	- 306	306
3	260– 320	60	120	290	6600	3000		27	- 150	150
4	320– 380	↓	130	350	↓	↓		31	- 129	129
5	380– 440		138	410				35	- 112	112
6	440– 500		140	470				↓	↓	↓
7	500– 560		↓	530						
8	560– 620	60		590	6600	3000			- 112	112
9	620– 682	62		652	12400	5600			- 212	1250
10	682– 744	62		714	12400	5600			- 212	1250
11	744– 805	61		775	12200	5600			- 212	1250
12	805– 862	57	↓	832	6850	2900			- 125	125
13	862– 919	57	140	889	6850	2900			- 125	125
14	919– 989	70	130	959	7000	3500			- 110	110
15	989–1059	↓	120	1029	↓	↓		35	- 110	110
16	1059–1129		114	1099				29	- 135	135
17	1129–1199		106	1169			↓	22	- 184	184
18	1199–1269	↓	90	1239	↓	↓	3	15	- 290	290
19	1269–1339	70	74	1309	7000	3500	2	9	- 500	500
20	1339–1410	71	66	1379	3500	1750	2	4	- 875	875

FIG. 5 FUSELAGE UNDERSTRUCTURE STIFFNESS DATA

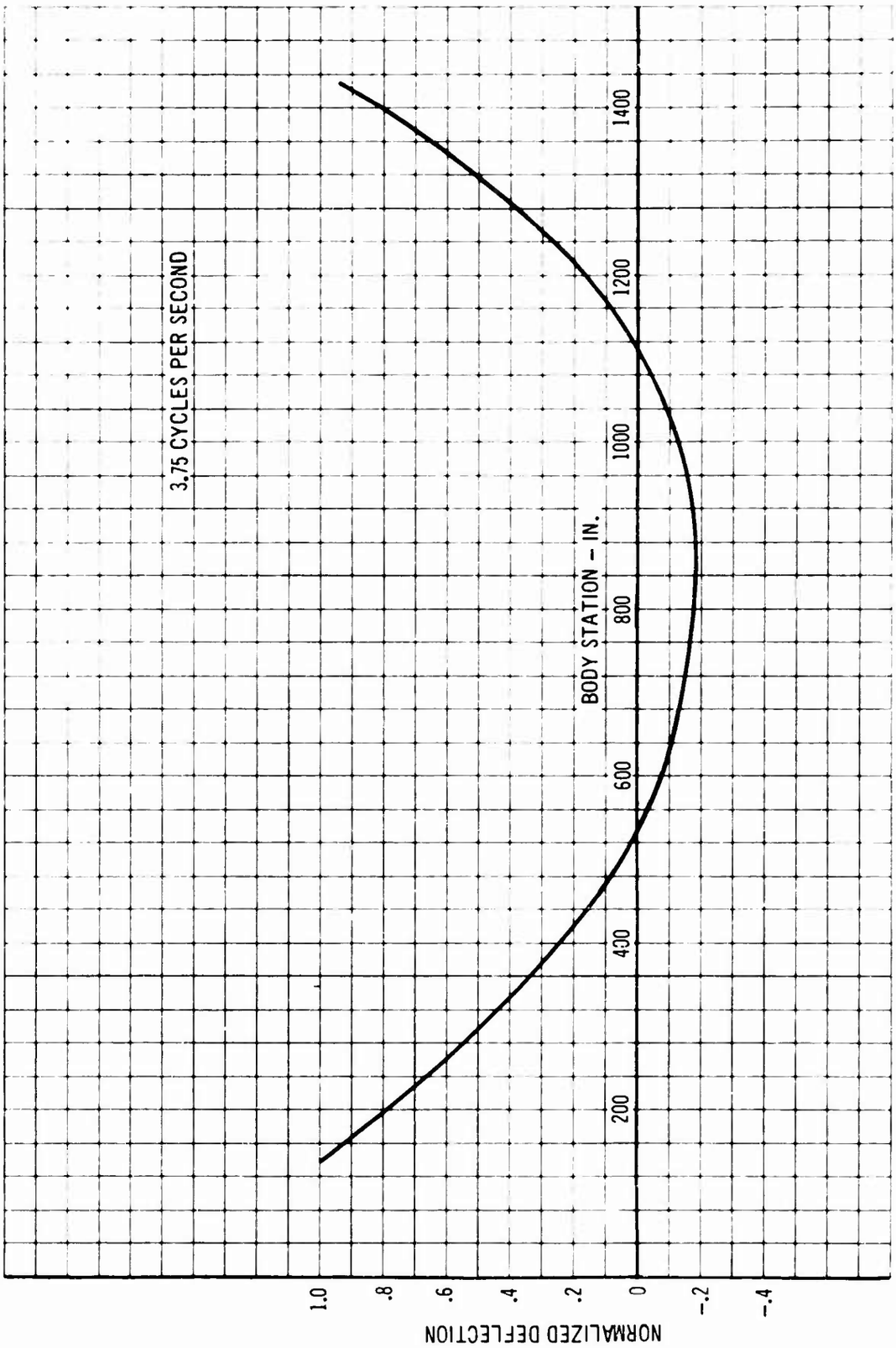

FIG. 6 FUSELAGE FIRST UNRESTRAINED VERTICAL BENDING MODE SHAPE

4.0 RESULTS

This section is divided into three main subsections. The first presents the results of the rigid body analyses, and the second those of analyses considering the longitudinal and vertical bending flexibilities of the airplane. The third subsection discusses the effects of variations in important analysis parameters.

4.1 RIGID BODY ANALYSES

Because it was believed from the beginning of these analyses that the rigid body motions would dominate, it was decided to present the rigid body results separately from those results where the longitudinal and vertical bending flexibilities of the fuselage were included. In the rigid body analysis the only motions considered were those of airplane center of gravity horizontal and vertical translation, and airplane pitch about the center of gravity.

Figs. 7 through 10 show the acceleration versus time histories during the 6 degree ramp crash determined using the rigid body equations of Section 2.1. Accelerations normal and parallel to the fuselage cabin floor at Body Stations 180, 682, and 1176 are given for initial impact velocities of 140, 160, 180, and 200 feet per second. A summary plot showing peak normal accelerations for each velocity and time at which the peaks occur is contained in Fig. 11.

The basic mechanism of the crash is illustrated in Fig. 12. In this figure, airplane position is plotted against normal acceleration at the center of gravity and airplane velocity parallel to the ramp surface. At time zero the airplane impacts the ramp approximately 30 feet from the ramp's base at 180 feet per second. The longitudinal axis of the airplane is parallel to the horizontal. At impact a force is quickly developed at the nose of the fuselage which causes the airplane to pitch up sharply, and this is reflected in the initial acceleration peaks at a time after impact of 0.08 seconds. The aircraft fuselage is now pitching into the ramp, and finally at a time of approximately 0.24 seconds, the entire fuselage forward of the trailing edge of the wing impacts. At this point, the peak accelerations of the 6 degree ramp crash occur. Because of the upward curvature of the aft portion of the fuselage, the aft body does not contact the ramp surface until after the peak accelerations have passed. The crushing of the aft fuselage is reflected by the gradual decrease of the acceleration from its maximum value.

Note that the velocity of the airplane after 0.7 seconds is only 25 feet per second less than at impact. It is estimated that it will take approximately 0.7 seconds after initial impact for the airplane nose to reach the top of the 6 degree ramp.

As can be seen by a study of the acceleration plots, the behavior of the airplane after impact is much the same for all velocities. The most significant differences appear to be that as the velocity increases, the peak accelerations increase and the time at which they occur decreases. This trend is illustrated clearly by Fig. 11.

INITIAL CONDITIONS - RIGID BODY			
SPEED	140 FT./SEC.	C.G. LOCATION- BODY STA.	682
ANGLE OF IMPACT	6 DEGREES	PLOWING COEFFICIENT	80 LB./IN.^{2}
WEIGHT	124,500 LBS.	PLOWING AREA	700 IN.^{2}
INERTIA ABOUT C.G.	4.64×10^9 LB./IN.^{2}	FRICTION COEFFICIENT	.3

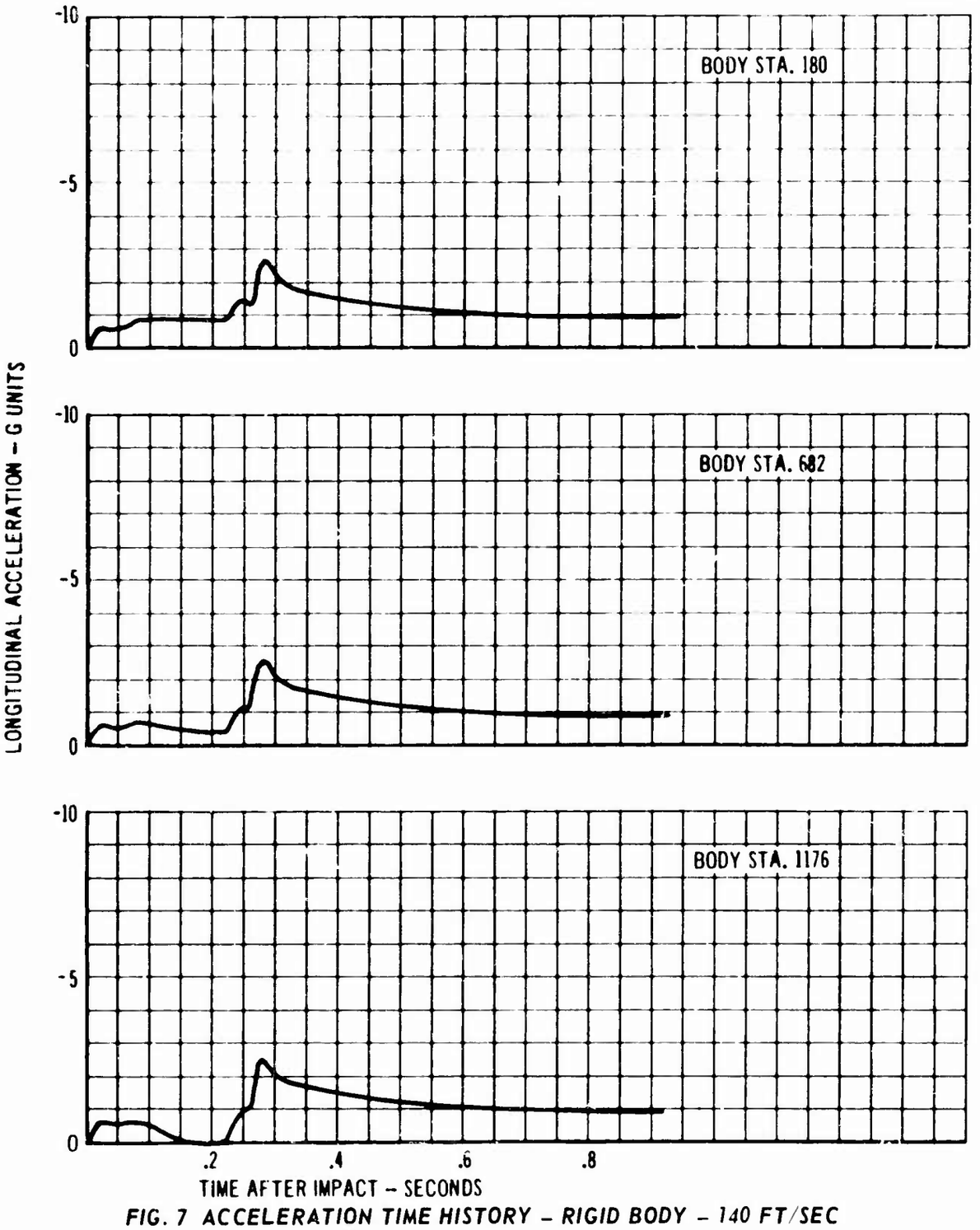

FIG. 7 ACCELERATION TIME HISTORY - RIGID BODY - 140 FT/SEC

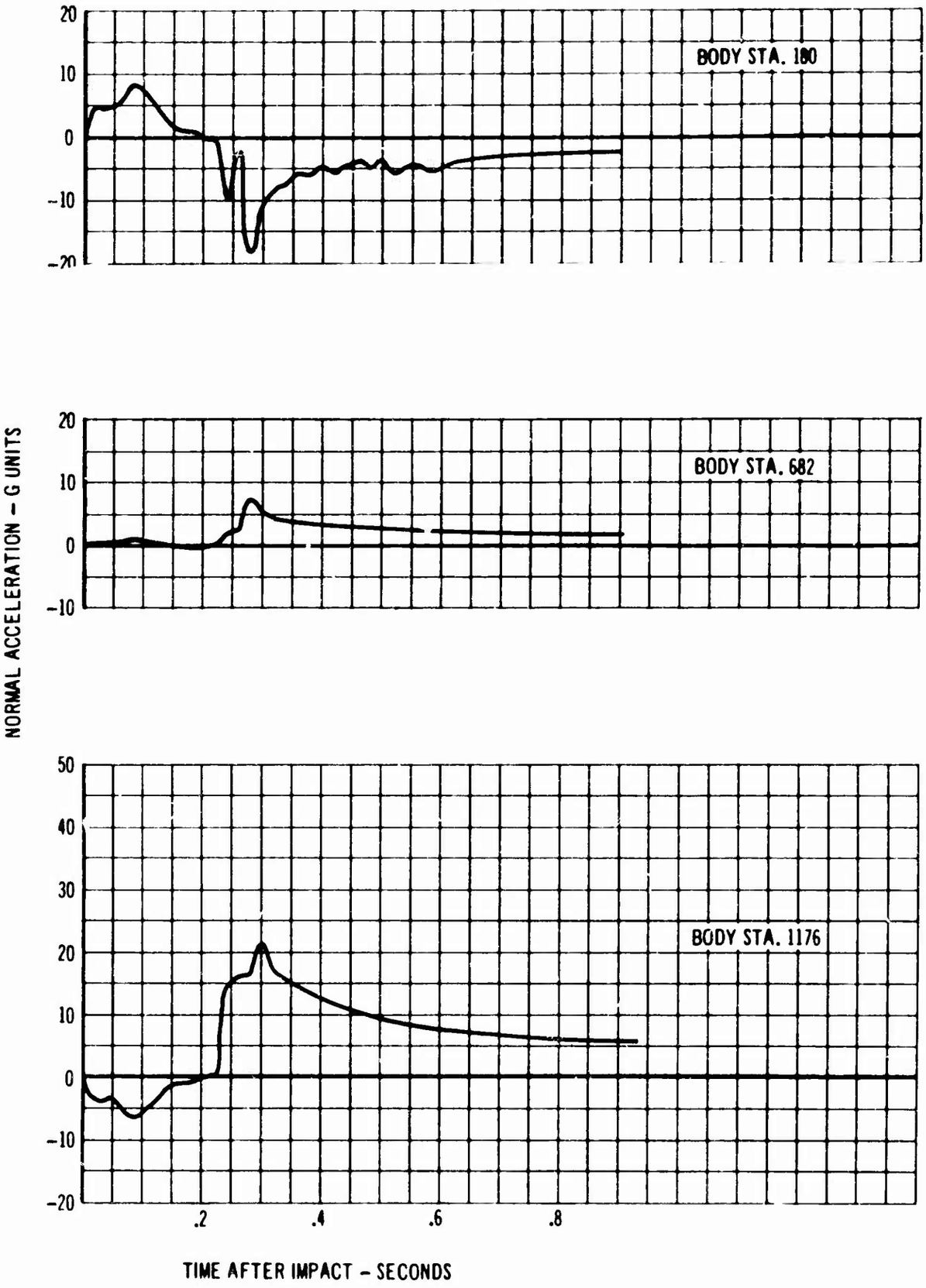

FIG. 7 ACCELERATION TIME HISTORY – RIGID BODY – 140 FT/SEC (continued)

INITIAL CONDITIONS - RIGID BODY			
SPEED	160 FT./SEC.	C.G. LOCATION - BODY STA.	682
ANGLE OF IMPACT	6 DEGREES	PLOWING COEFFICIENT	80LB./IN.^{2}
WEIGHT	124,500 LBS.	PLOWING AREA	700 IN.^{2}
INERTIA ABOUT C.G.	4.64x10^{9}LB./IN.^{2}	FRICTION COEFFICIENT	.3

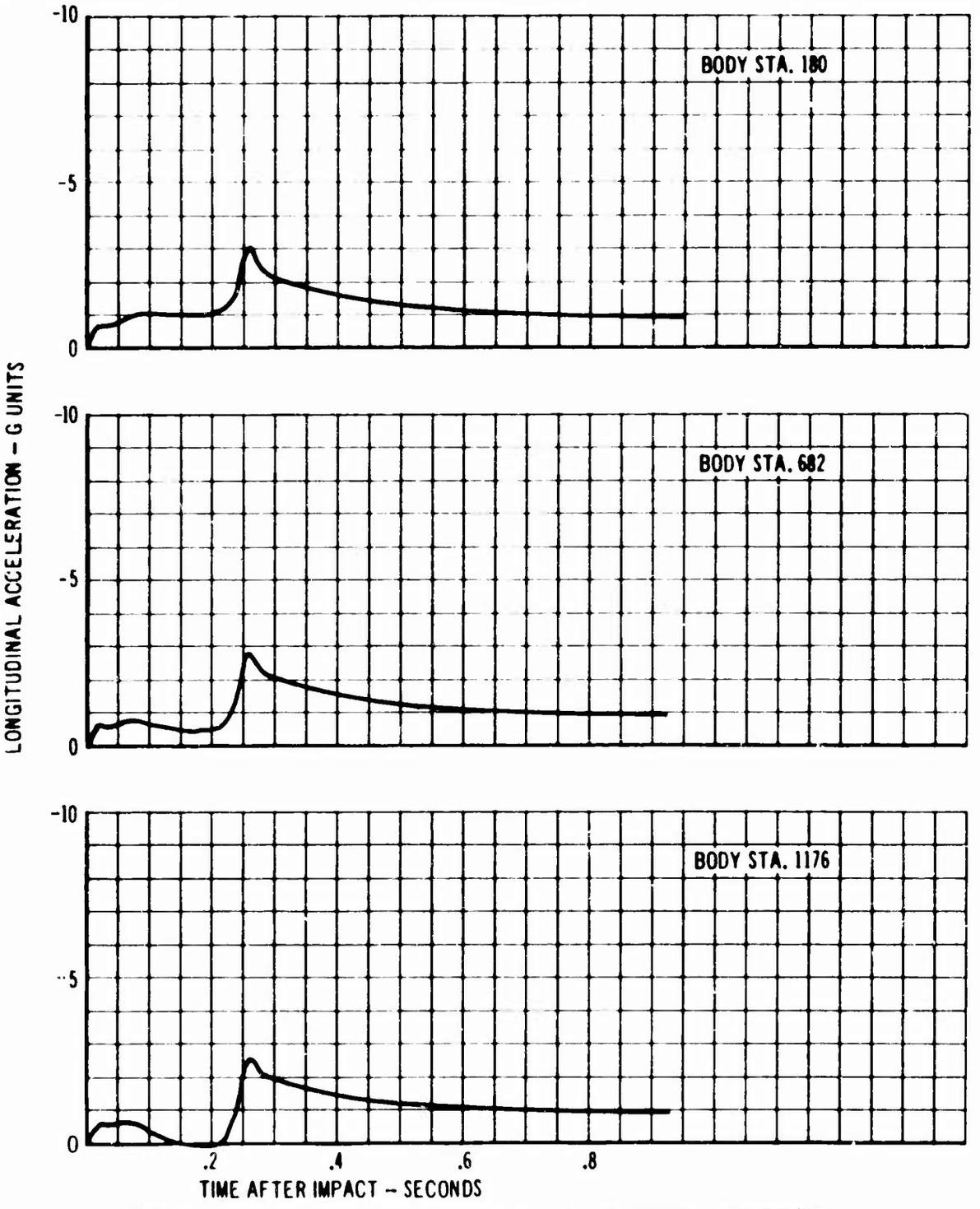

FIG. 8 ACCELERATION TIME HISTORY - RIGID BODY - 160 FT/SEC

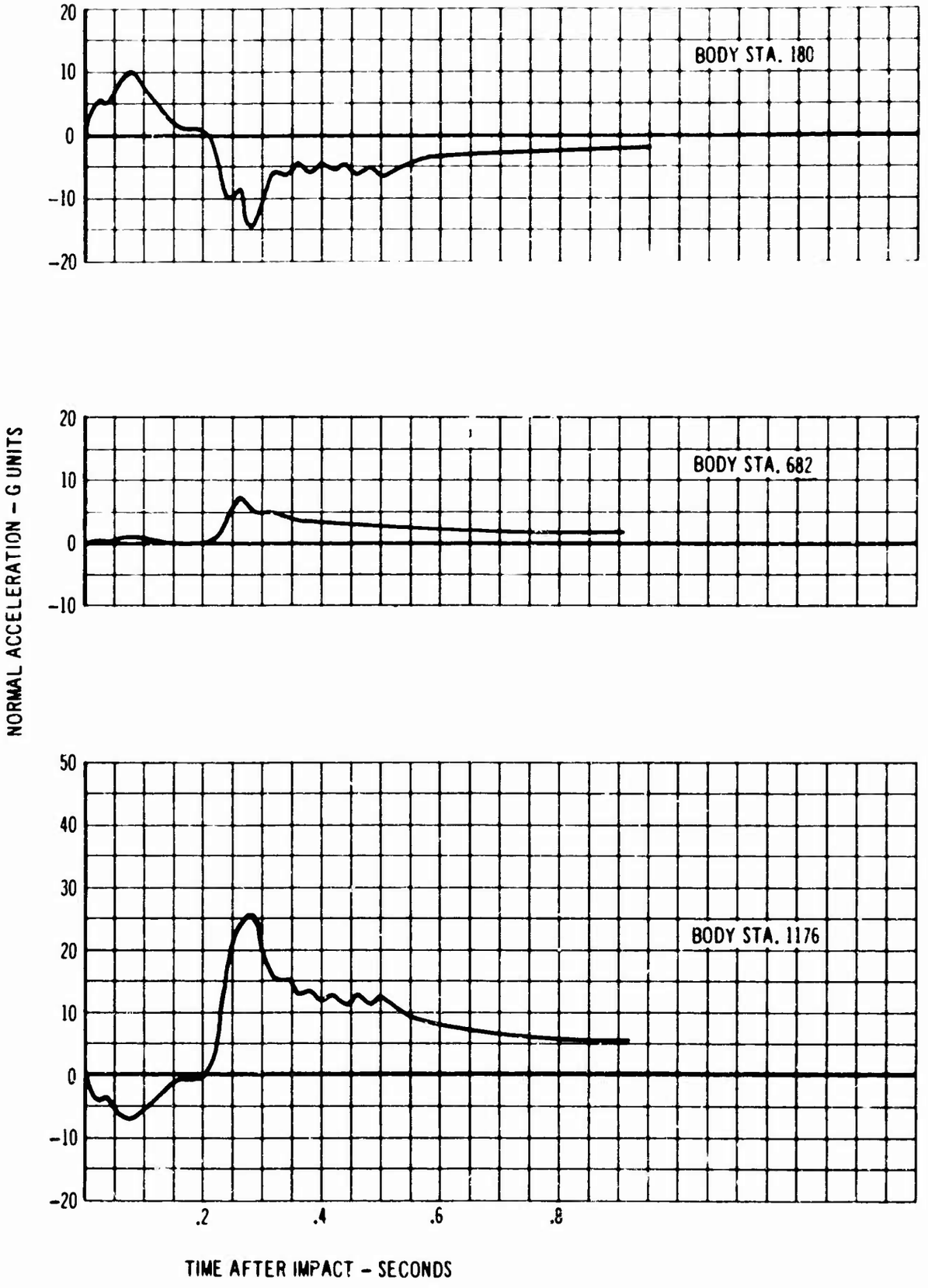

FIG. 8 ACCELERATION TIME HISTORY – RIGID BODY 160 FT/SEC (continued)

INITIAL CONDITIONS - RIGID BODY			
SPEED	180 FT./SEC.	C.G. LOCATION - BODY STA.	682
ANGLE OF IMPACT	6 DEGREES	PLOWING COEFFICIENT	80 LB./IN.^{2}
WEIGHT	124,500 LBS.	PLOWING AREA	700 IN.^{2}
INERTIA ABOUT C.G.	4.64×10^9 LB./IN.^{2}	FRICTION COEFFICIENT	.3

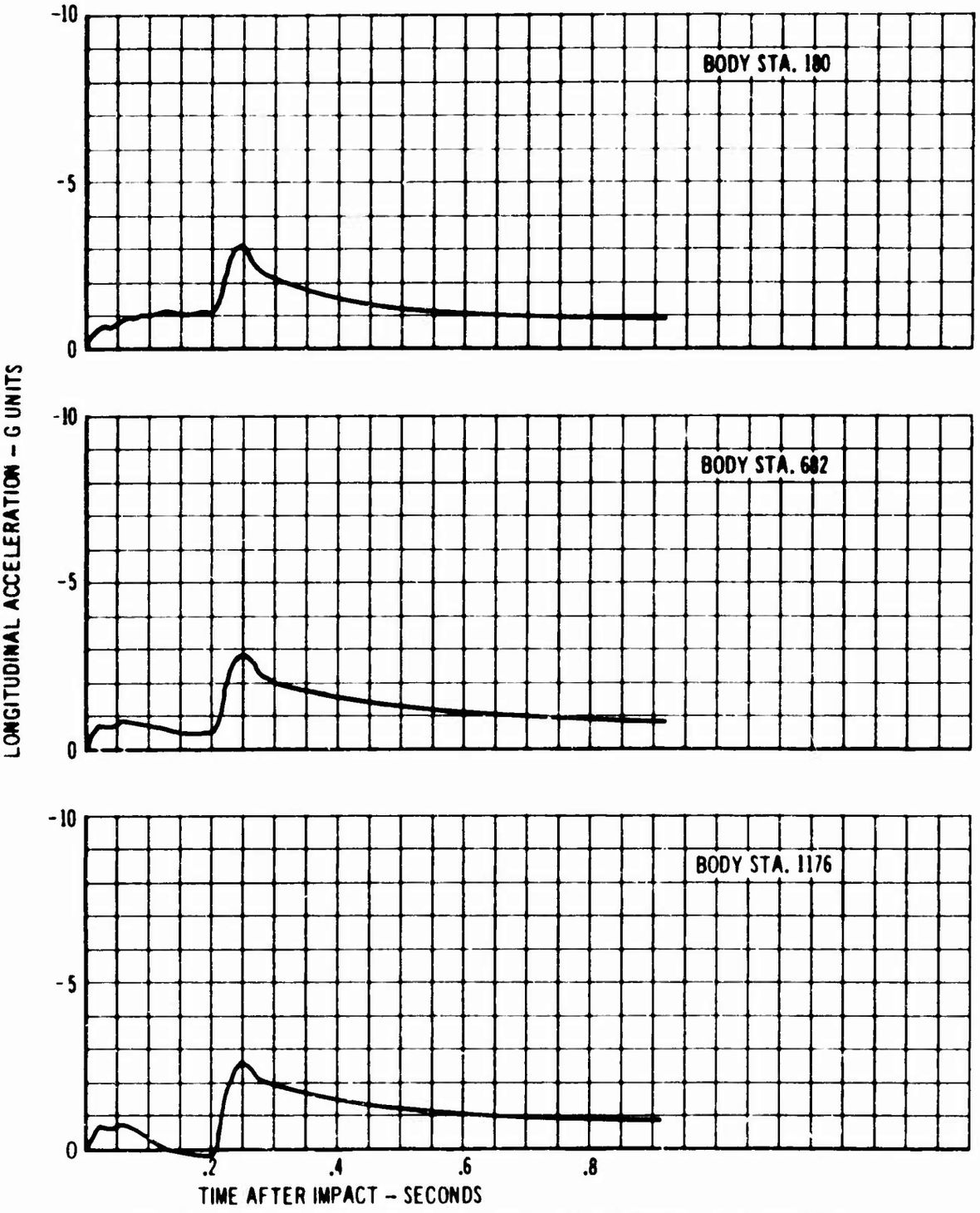

FIG. 9 ACCELERATION TIME HISTORY - RIGID BODY - 180 FT/SEC

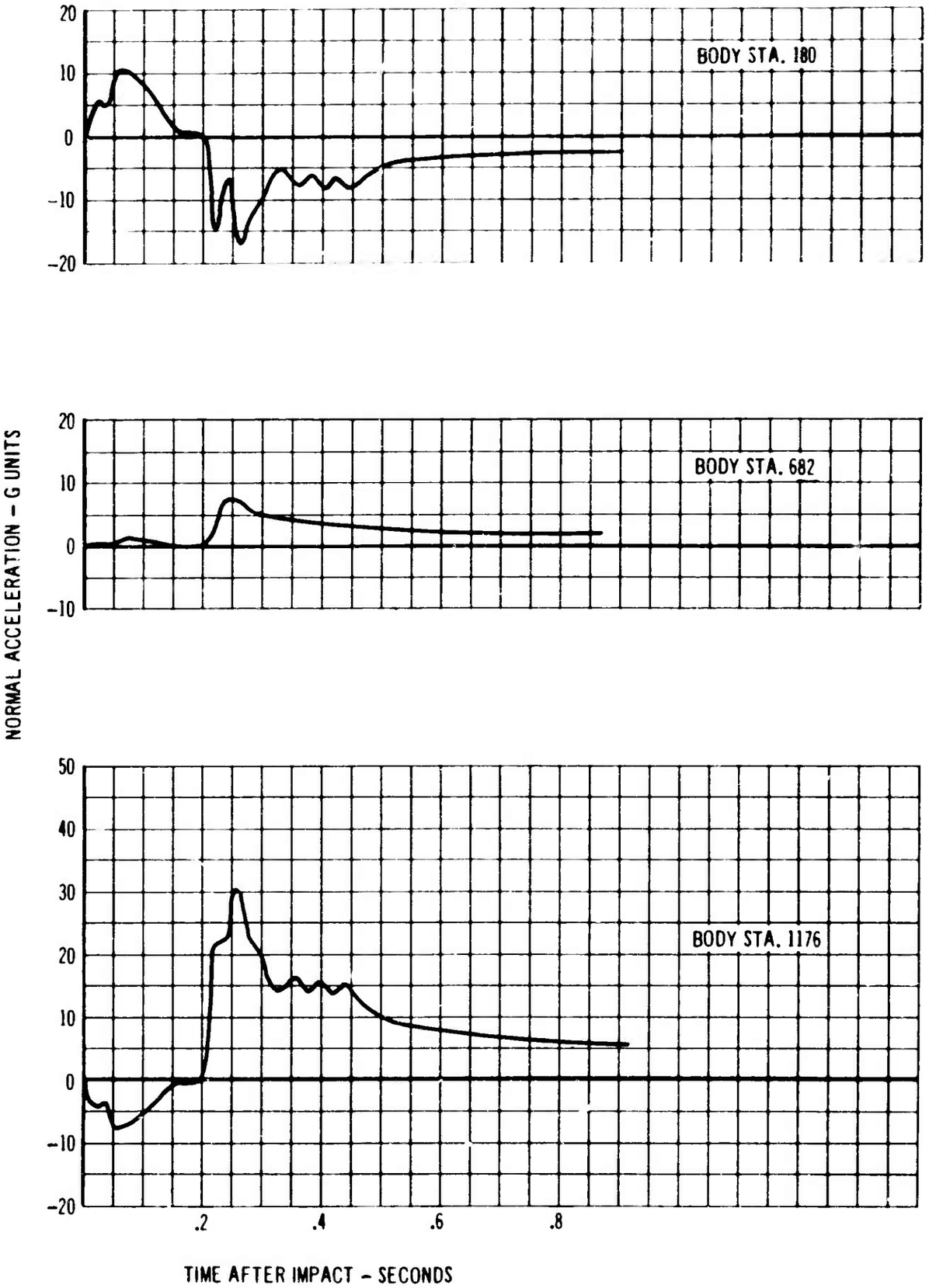

FIG. 9 ACCELERATION TIME HISTORY – RIGID BODY – 180 FT/SEC (continued)

INITIAL CONDITIONS - RIGID BODY			
SPEED	200 FT./SEC.	C.G. LOCATION-BODY STA.	682
ANGLE OF IMPACT	6 DEGREES	PLOWING COEFFICIENT	80LB./IN.^{2}
WEIGHT	124,500 LBS.	PLOWING AREA	700 IN.^{2}
INERTIA ABOUT C.G.	4.64×10^9 LB./IN.^{2}	FRICTION COEFFICIENT	.3

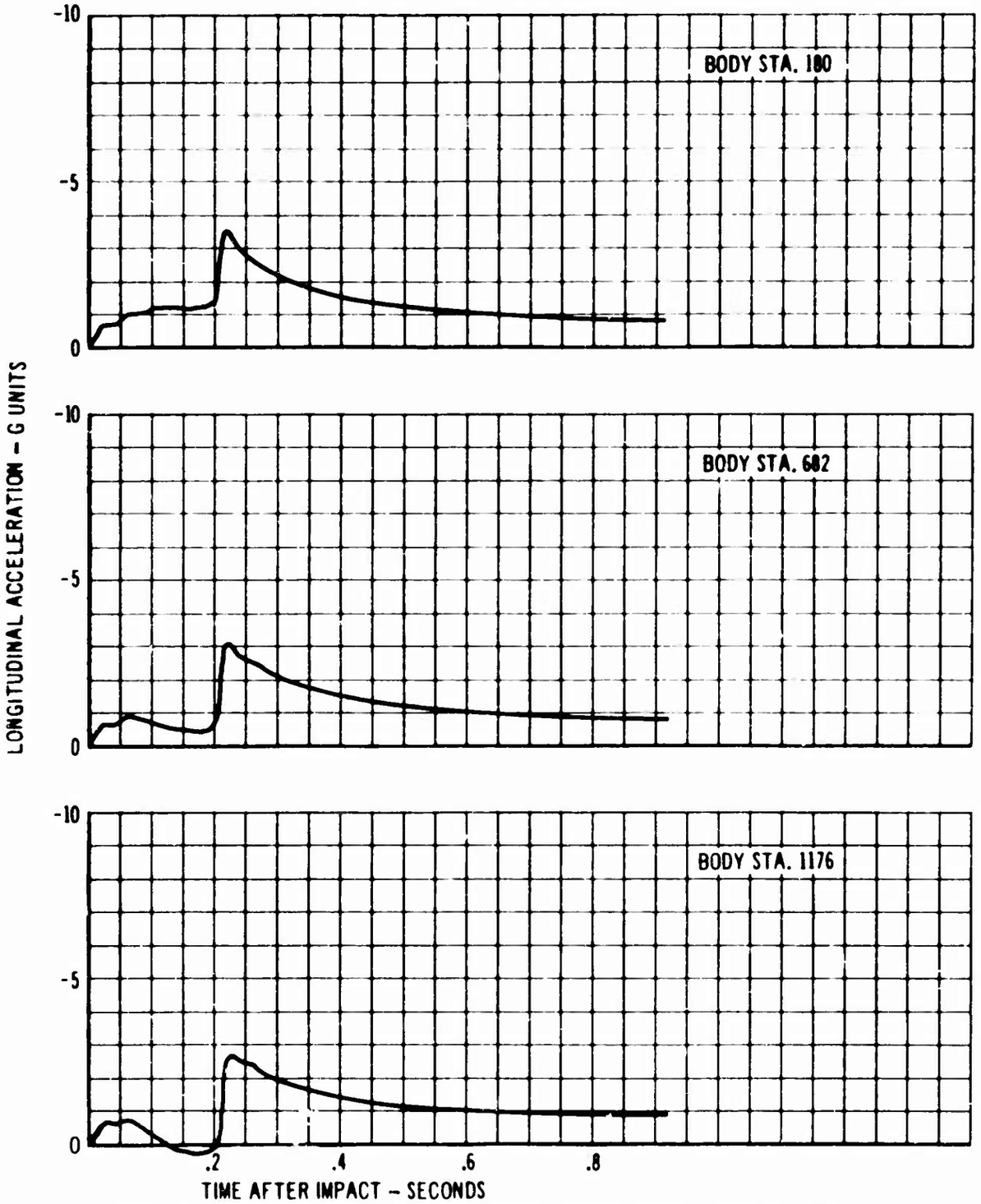

FIG. 10 ACCELERATION TIME HISTORY - RIGID BODY - 200 FT/SEC

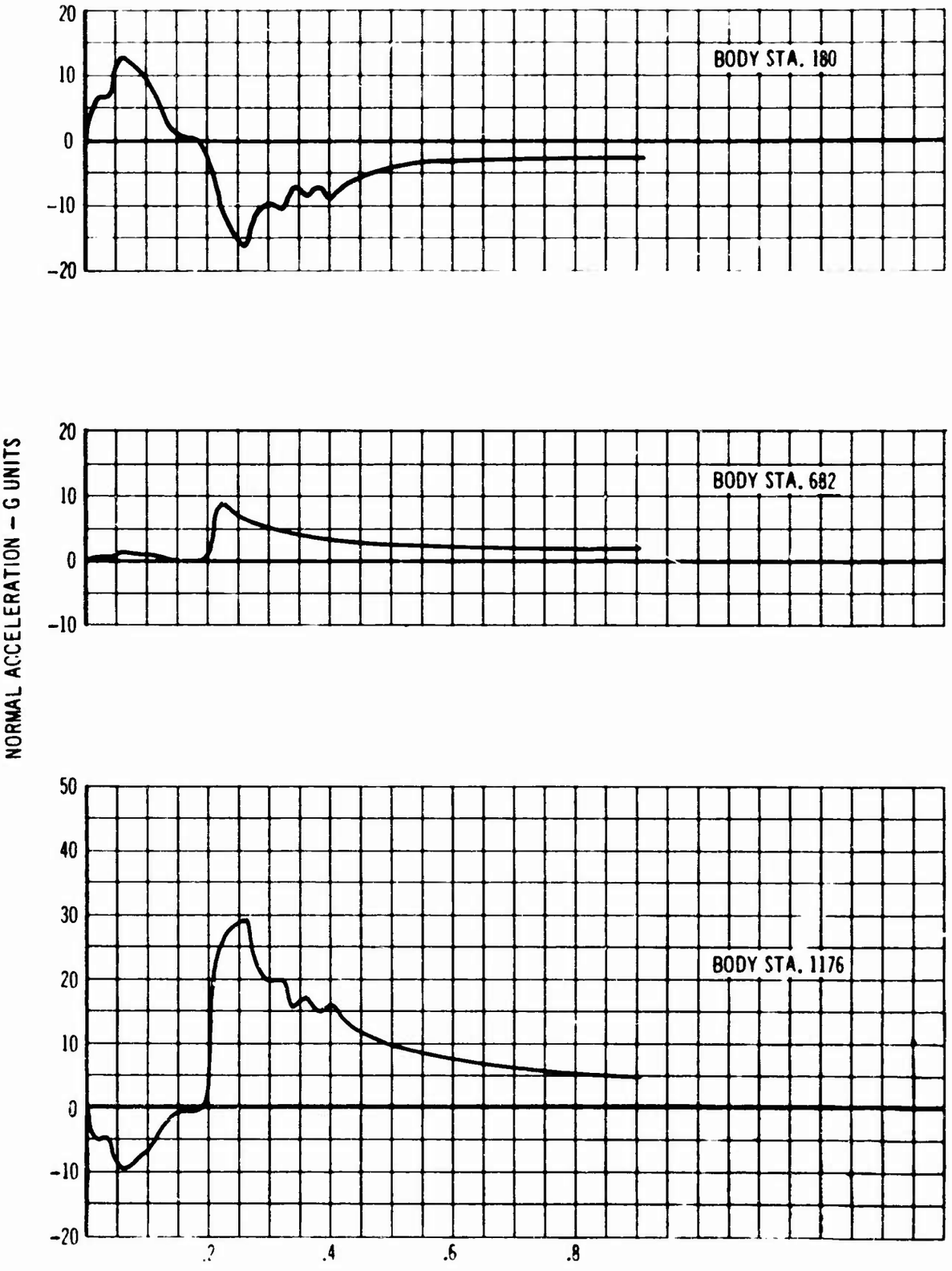

FIG. 10 ACCELERATION TIME HISTORY – RIGID BODY – 200 FT/SEC (continued)

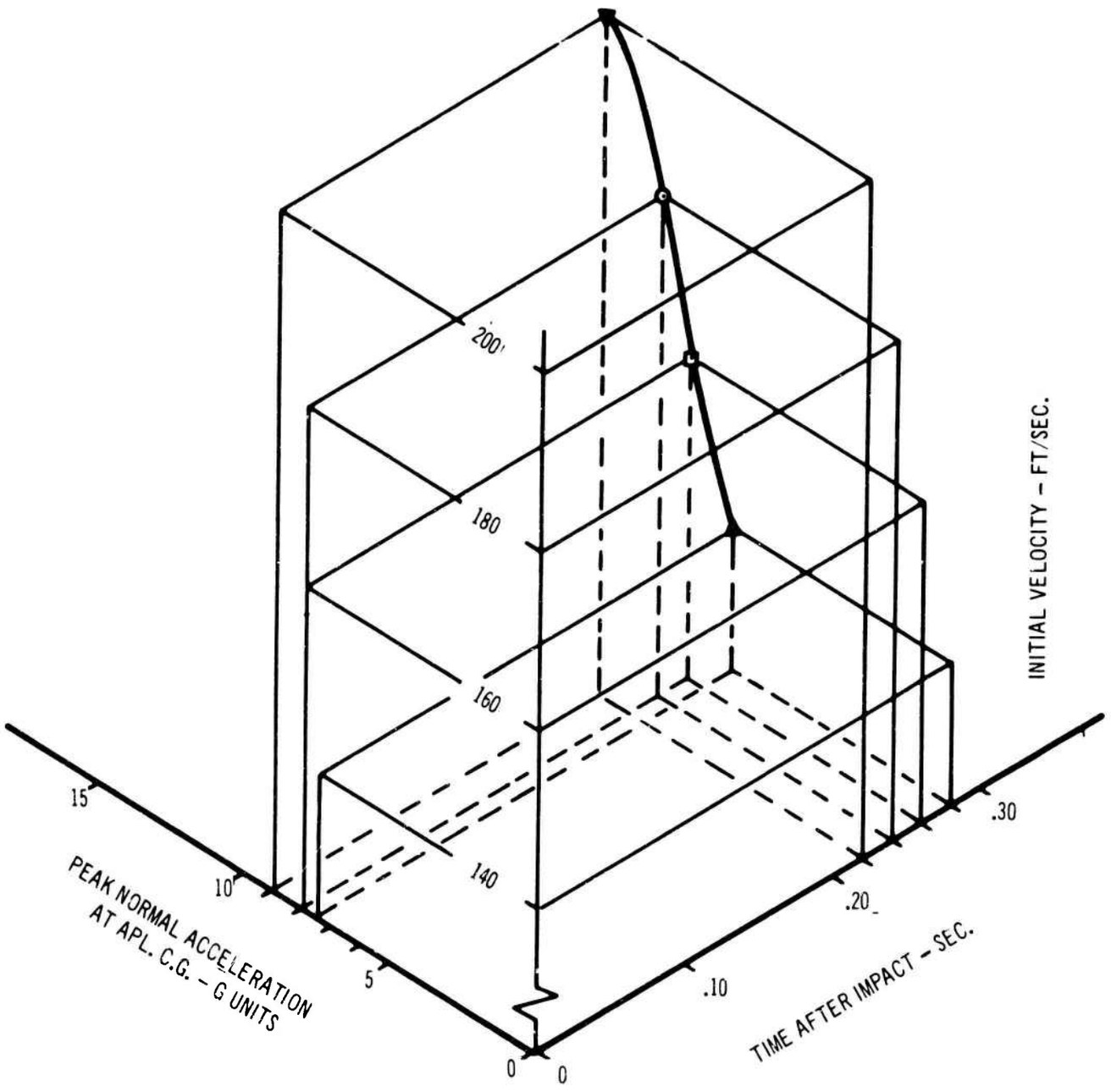

FIG. 11 ACCELERATION-TIME-VELOCITY SUMMARY - RIGID BODY

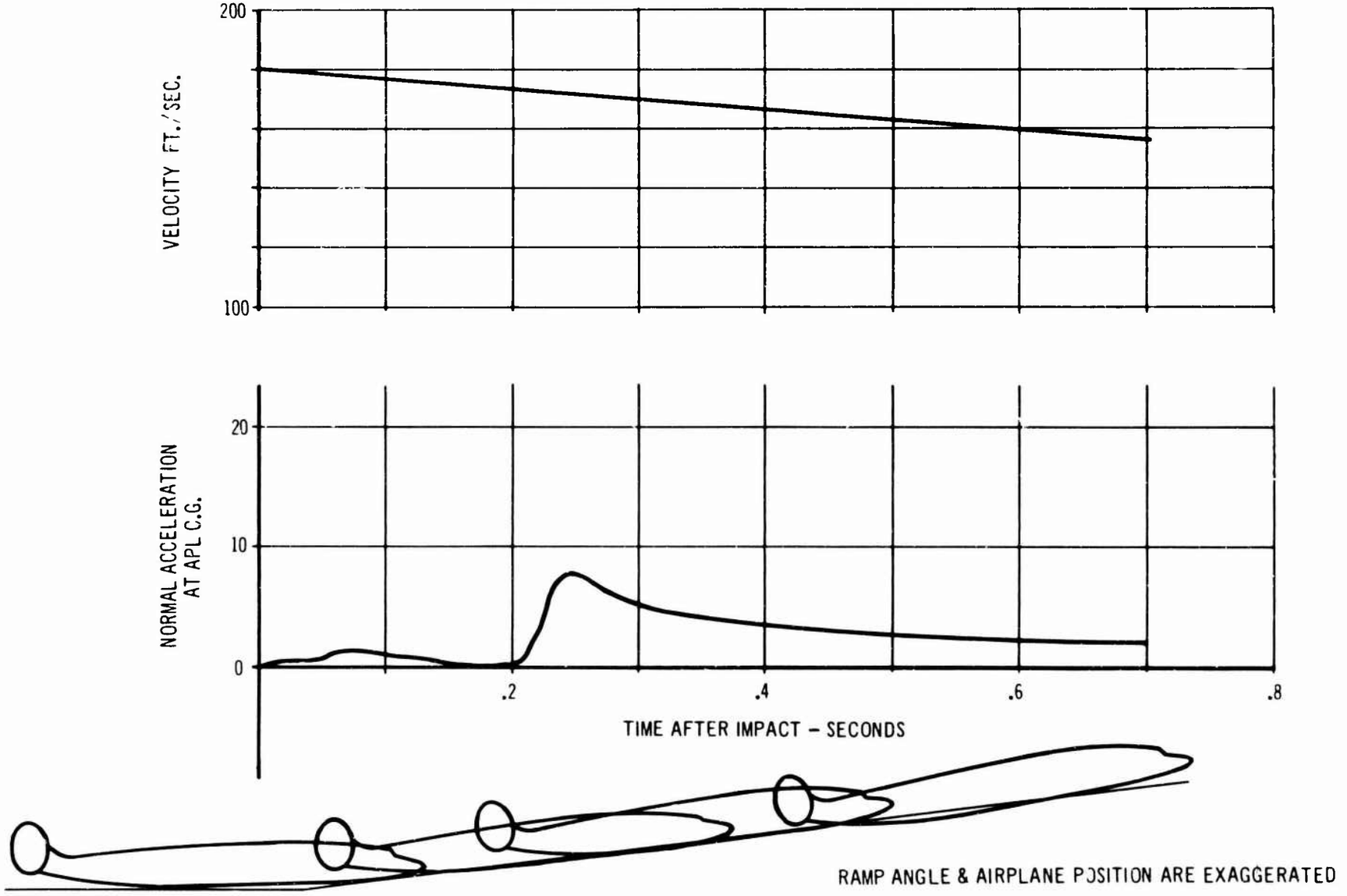

FIG. 12 TRAJECTORY-TIME – VELOCITY SUMMARY – 180 FT/SEC

An additional interpretation of the results can be made in terms of what passengers or crew seated at Body Stations 180, 682, and 1176 would feel during the 6 degree ramp crash. For example, Figs. 7 through 10 indicate that at Body Station 180, a passenger at initial impact would be thrown forward and downward into his seat, while a passenger at Body Station 1176 would be accelerated forward and upward. At the airplane center of gravity, Body Station 682, the passengers would experience a slight downward and forward acceleration.

At peak G's at an approximate time of 0.22 seconds, passengers at all stations would experience maximum forward accelerations. Those passengers at Body Stations 682 and 1176 would be thrown downward into their seats while those in the nose at Body Station 180 would be accelerated upward with considerable force. It would appear that because the airplane is pitching about its center of gravity, passengers seated at or just forward of the airplane center of gravity would experience the least overall forces during the crash.

4.2 FLEXIBLE BODY ANALYSES

In a symmetric crash, as is being considered here, fuselage longitudinal and vertical bending vibrations might modify the rigid body results significantly. Accordingly, the equations of Section 2.0 were used to obtain acceleration time histories similar to those for the rigid body analysis. In Figs. 13 through 16 accelerations normal and parallel to the fuselage cabin floor at Body Stations 180, 682, and 1176 are given for initial impact velocities of 140, 160, 180, and 200 feet per second. A summary plot of peak normal G's at the airplane center of gravity versus time after impact is shown in Fig. 17.

In general, introduction of the fuselage vertical bending and longitudinal flexibility into the problem had little direct effect on the answers. The rigid body accelerations tended to control the results. One significant difference that is noted is in the normal acceleration peaks at the nose and tail at a time after impact of approximately 0.08 seconds. Analysis indicates that the nose and tail at initial impact tend to bend upward relative to the relatively rigid center body at the wing fuselage juncture. This does not significantly affect the normal accelerations at the center of gravity, but it does decrease the initial normal accelerations at the tail and causes the normal acceleration peak at Body Station 180, which occurs 0.08 seconds after impact in the rigid body analysis, to shift to 0.03 seconds.

4.2.1 Fuselage Failure

Fig. 18 shows, plotted against impact velocity, maximum fuselage bending deflections at the nose during initial impact. All maximum deflections occurred 0.14 seconds after impact. An estimate of the ultimate strength of the fuselage indicates that a bending deflection of approximately 5-8 inches at the nose would be sufficient to fail the fuselage in the neighborhood of the forward spar of the wing at the wing-body juncture. Therefore, although marginal at the lower velocities, it would appear that the 1649 fuselage will fail during the test. Since the analysis assumes the portion of the fuselage above the cabin floor remains intact during the 6 degree ramp crash, analytical results

beyond the time of failure will be questionable since the physical characteristics of the airplane will change. The degree to which the accuracy of the results is affected will depend on the type of failure that occurs.

4.3 PARAMETRIC VARIATIONS

The loads experienced by an aircraft during a crash are dependent on a number of parameters, many of which cannot always be determined or analytically represented with desired engineering accuracy. The most important of these are the following:

- Impact velocity
- Airplane geometry, weight, and inertia
- Ramp shape
- Friction force
- Plowing force
- Damping forces
- Ground stiffness

The relative effects of each of these parameters will be discussed individually in this section. All analyses accomplished for this section utilized only the rigid body equations.

4.3.1 Impact Velocity

The influence of initial impact velocity has already been discussed in Section 4.2. Figs. 11 and 17 most clearly illustrate how peak accelerations and the time at which they occur vary with increasing impact velocity. Generally, increasing the impact velocity causes higher peak accelerations at an earlier time after impact.

4.3.2 Airplane Geometry, Weight, and Inertia

Studies of the effect of variations of airplane weight and inertia on crash loads were not accomplished for the Lockheed 1649. However, some idea of the magnitude of the effects of airplane geometry, weight, and inertia can be gained by a study of Fig. 19. This presents the results of an analytical crash loads investigation of a Curtiss C-46, an airplane with a gross weight of approximately 30 percent that of the Constellation. * The initial conditions for the C-46 study were exactly the same as those for the 1649 investigation; that

* *This C-46 analysis was accomplished at an earlier date, and duplicates an experimental test conducted by the NACA as reported in Ref. 9.*

INITIAL CONDITIONS - FLEXIBLE BODY			
SPEED	140 FT./SEC.	C.G. LOCATION-BODY STA.	682
ANGLE OF IMPACT	6 DEGREES	PLOWING COEFFICIENT	80LB./IN.^{2}
WEIGHT	124,500 LBS.	PLOWING AREA	700 IN.^{2}
INERTIA ABOUT C.G.	4.64x10^{9}LB./IN.^{2}	FRICTION COEFFICIENT	.3

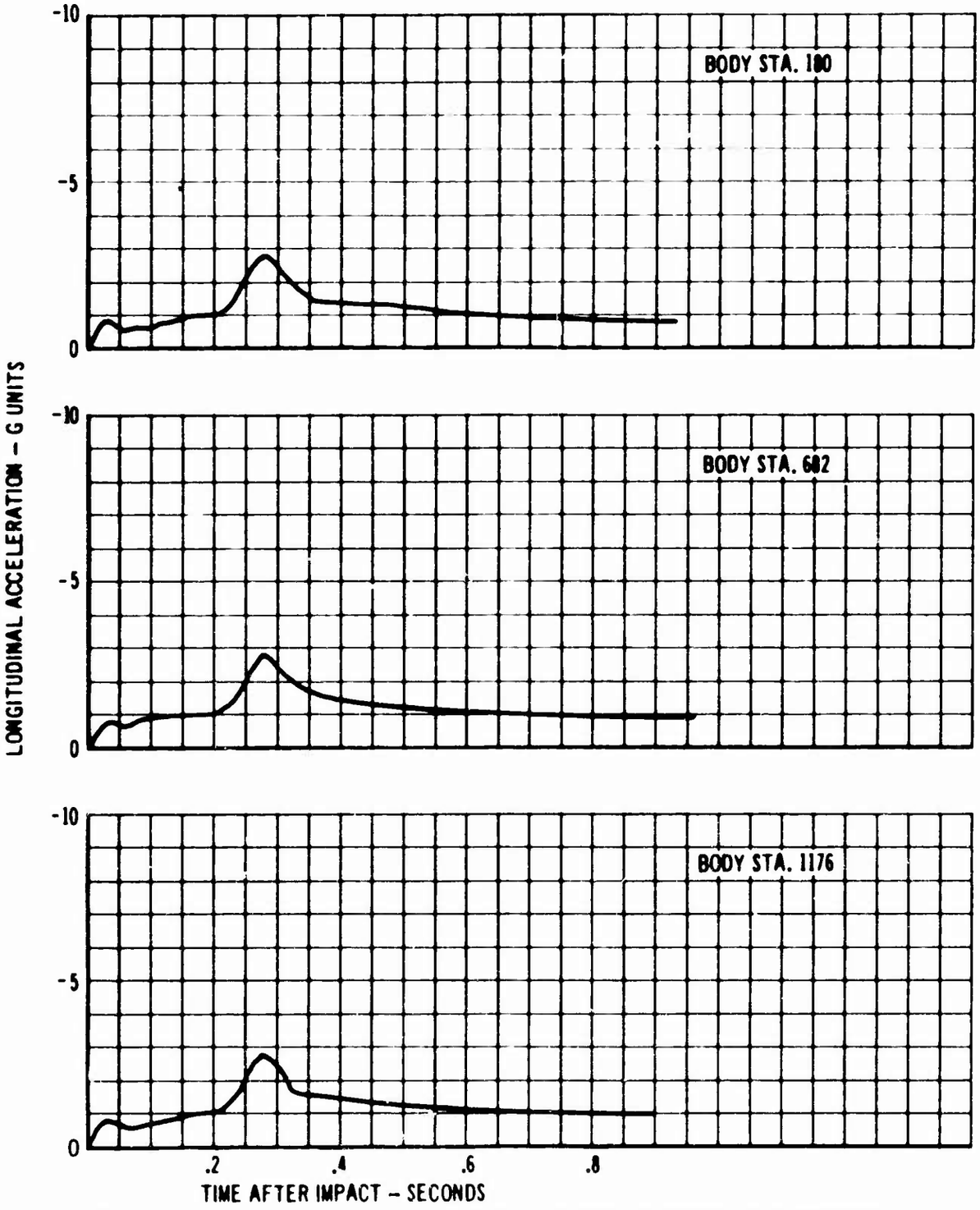

FIG. 13 ACCELERATION TIME HISTORY - FLEXIBLE BODY - 140 FT/SEC

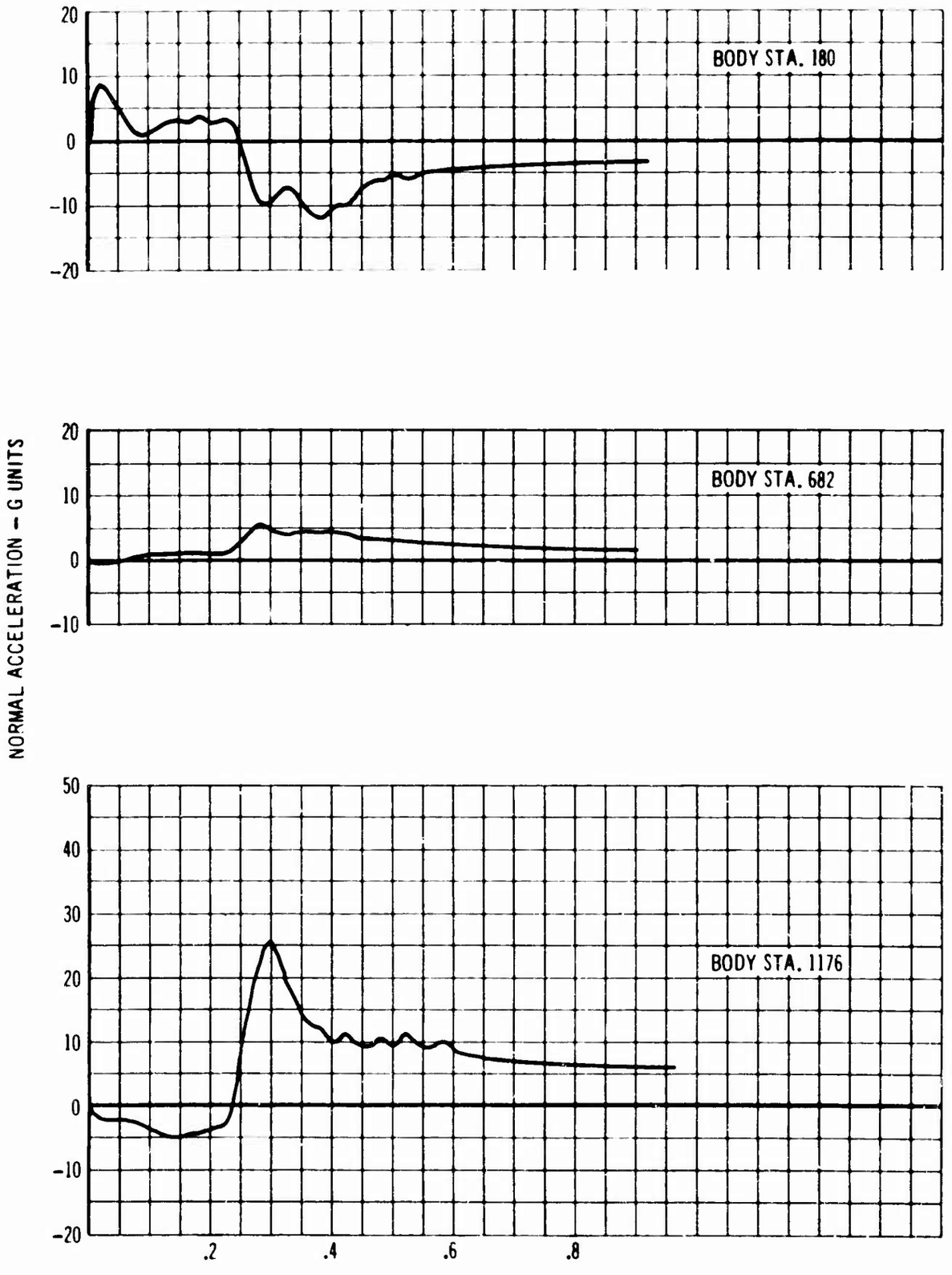

FIG. 13 ACCELERATION TIME HISTORY - FLEXIBLE BODY - 140 FT/SEC (continued)

INITIAL CONDITIONS - FLEXIBLE BODY			
SPEED	160 FT./SEC.	C.G. LOCATION- BODY STA.	682
ANGLE OF IMPACT	6 DEGREES	PLOWING COEFFICIENT	80LB./IN.^{2}
WEIGHT	124,500 LBS.	PLOWING AREA	700 IN.^{2}
INERTIA ABOUT C.G.	4.64x10^{9}LB./IN.^{2}	FRICTION COEFFICIENT	.3

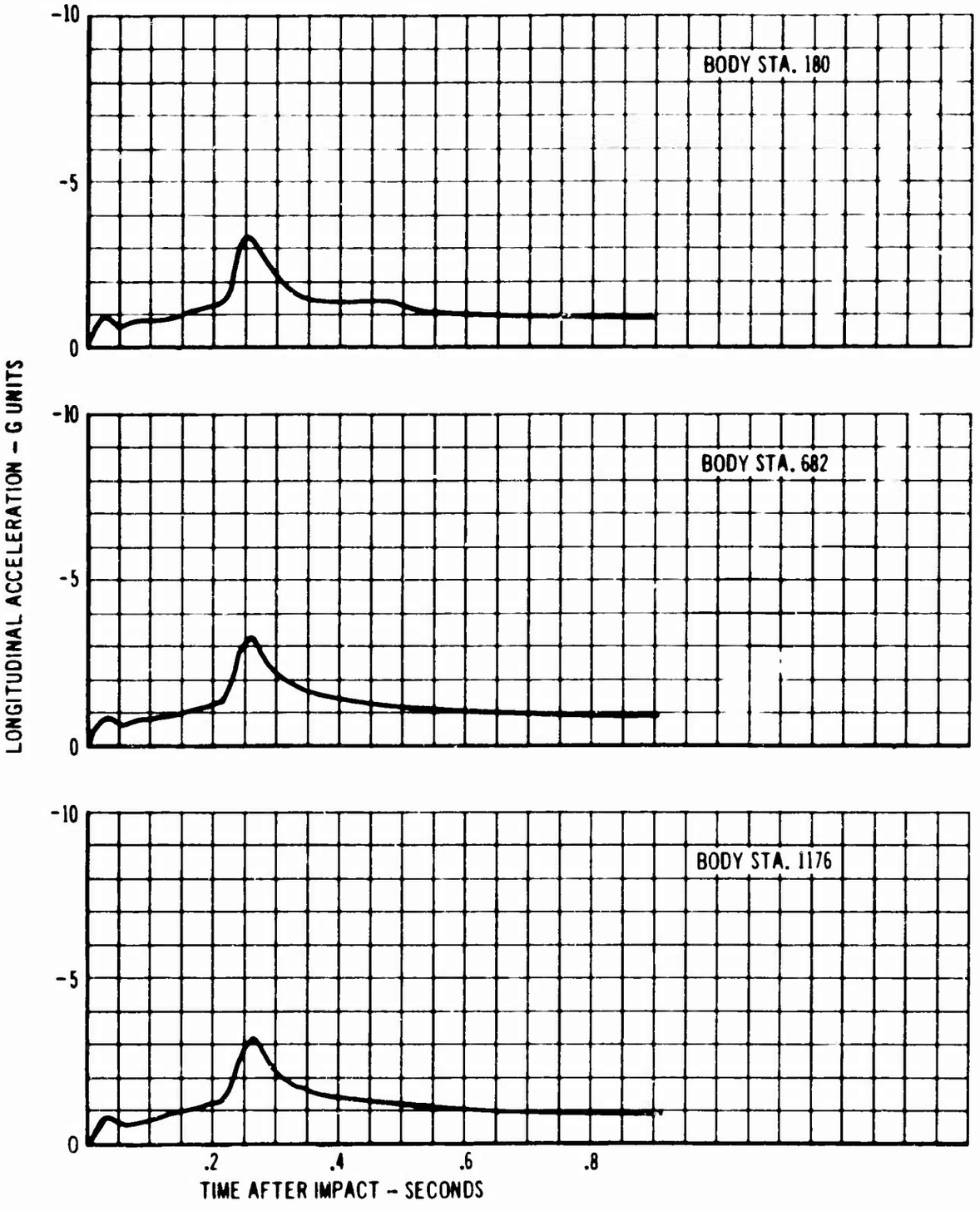

FIG. 14 ACCELERATION TIME HISTORY - FLEXIBLE BODY - 160 FT/SEC

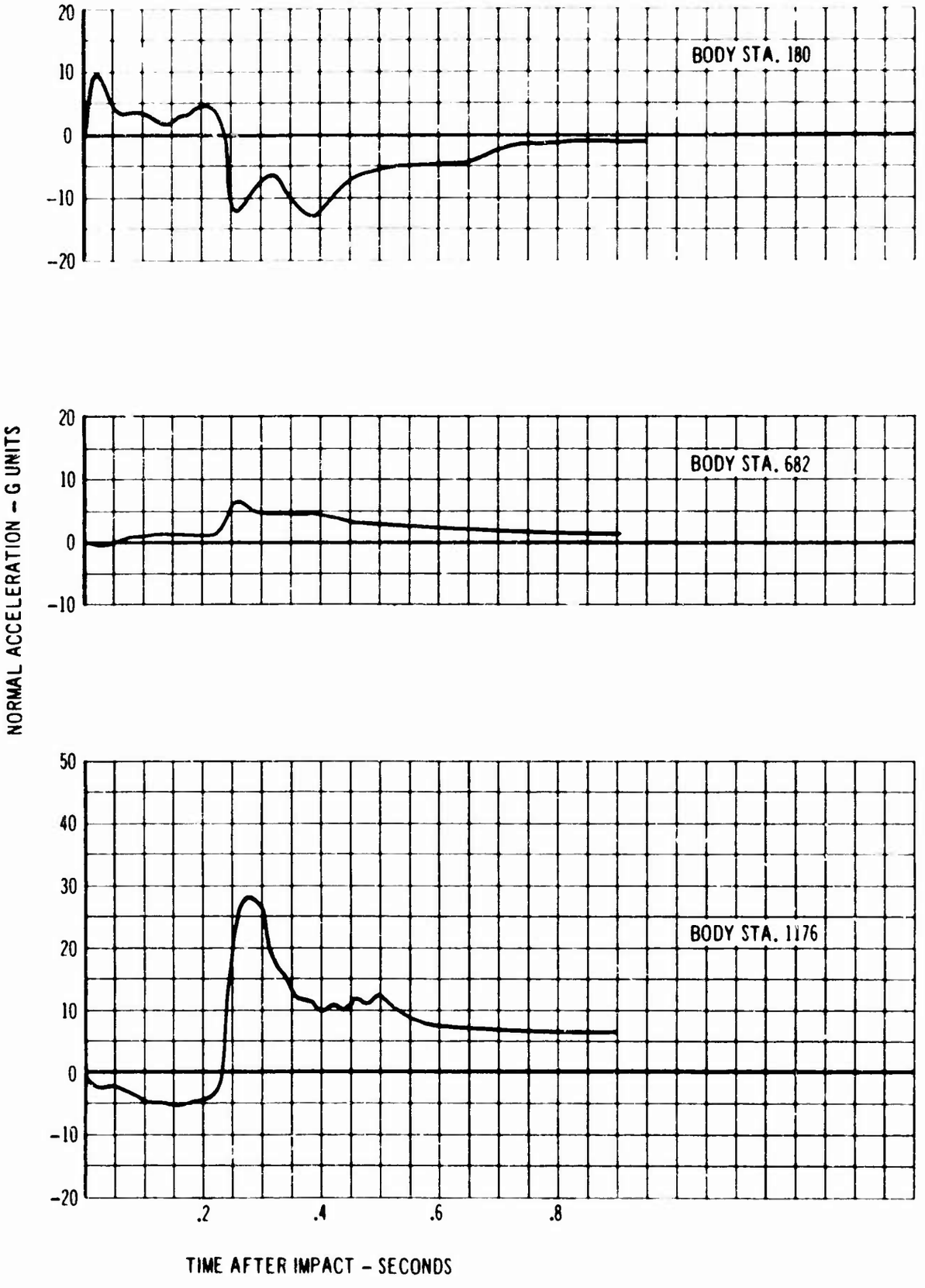

FIG. 14 ACCELERATION TIME HISTORY – FLEXIBLE BODY – 160 FT/SEC (continued)

INITIAL CONDITIONS - FLEXIBLE BODY			
SPEED	180 FT./SEC.	C.G. LOCATION-BODY STA.	682
ANGLE OF IMPACT	0 DEGREES	PLOWING COEFFICIENT	80 LB./IN.^{2}
WEIGHT	124,500 LBS.	PLOWING AREA	700 IN.^{2}
INERTIA ABOUT C.G.	4.64×10^9 LB./IN.^{2}	FRICTION COEFFICIENT	.3

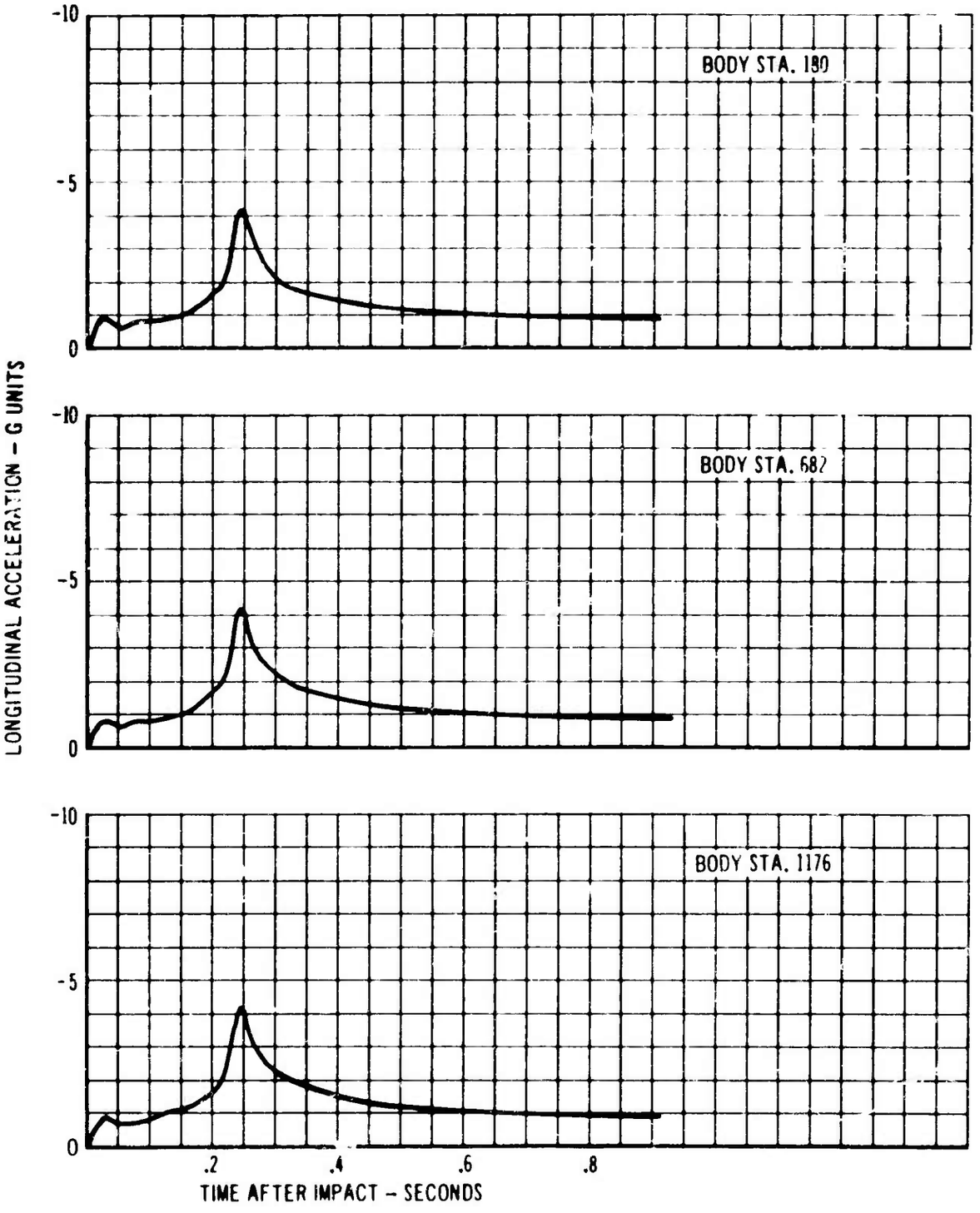

FIG. 15 ACCELERATION TIME HISTORY - FLEXIBLE BODY - 180 FT/SEC

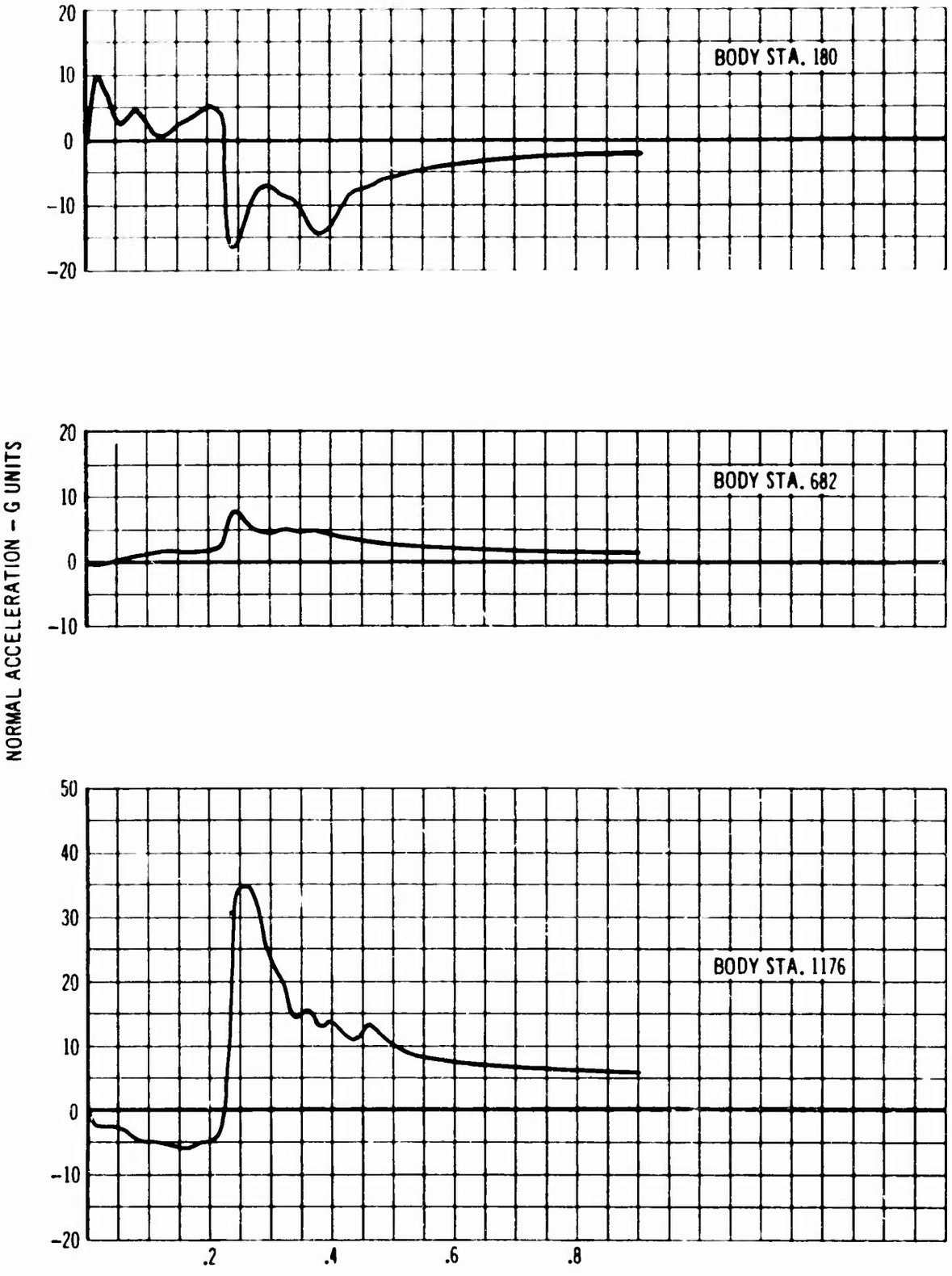

FIG. 15 ACCELERATION TIME HISTORY – FLEXIBLE BODY – 180 FT/SEC (continued)

INITIAL CONDITIONS - FLEXIBLE BODY			
SPEED	200 FT./SEC.	C.G. LOCATION-BODY STA.	682
ANGLE OF IMPACT	6 DEGREES	PLOWING COEFFICIENT	80 LB./IN.^{2}
WEIGHT	124,500 LB.	PLOWING AREA	700 IN.^{2}
INERTIA ABOUT C.G.	4.64×10^9 LB./IN.^{2}	FRICTION COEFFICIENT	.3

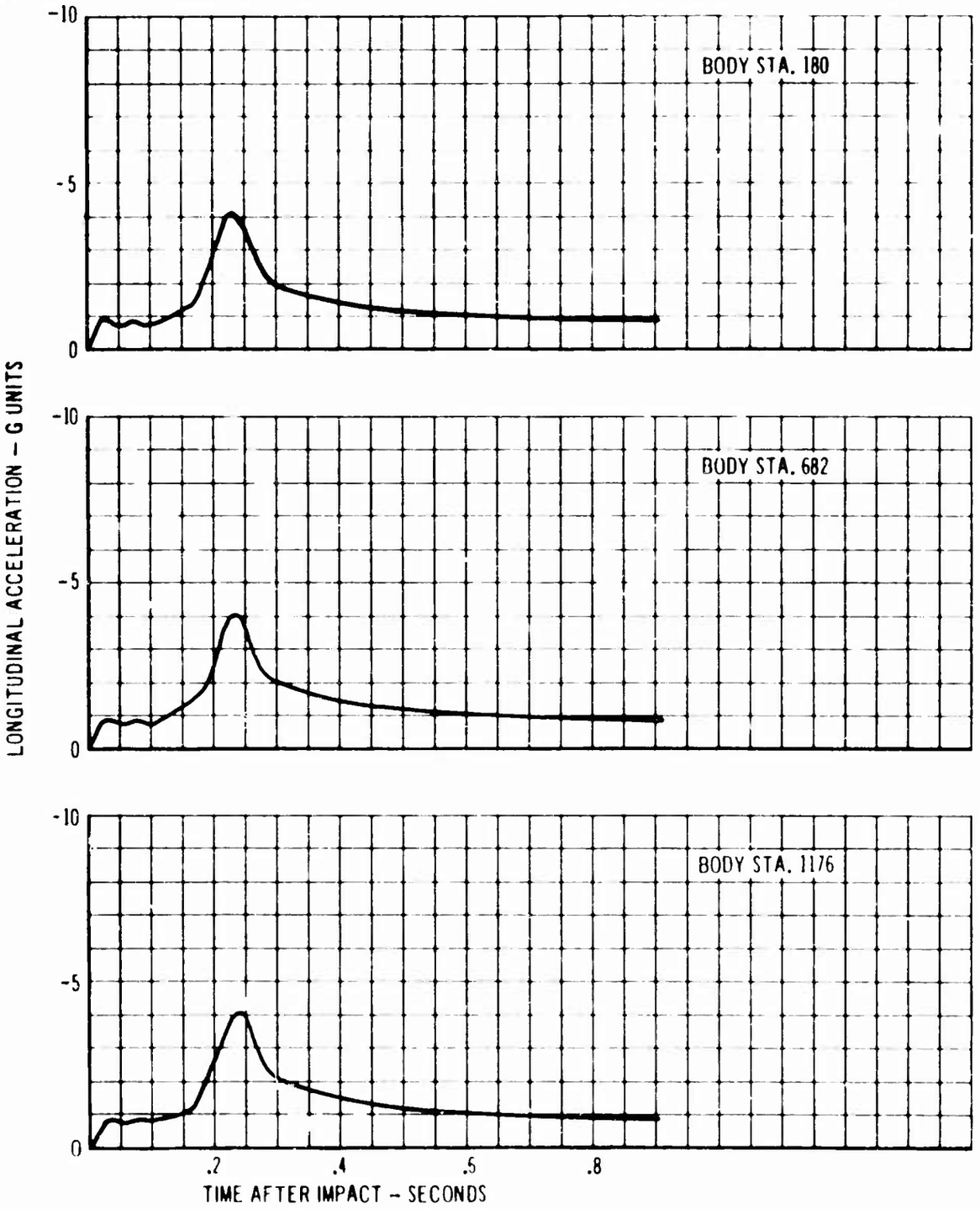

FIG. 16 ACCELERATION TIME HISTORY - FLEXIBLE BODY - 200 FT/SEC

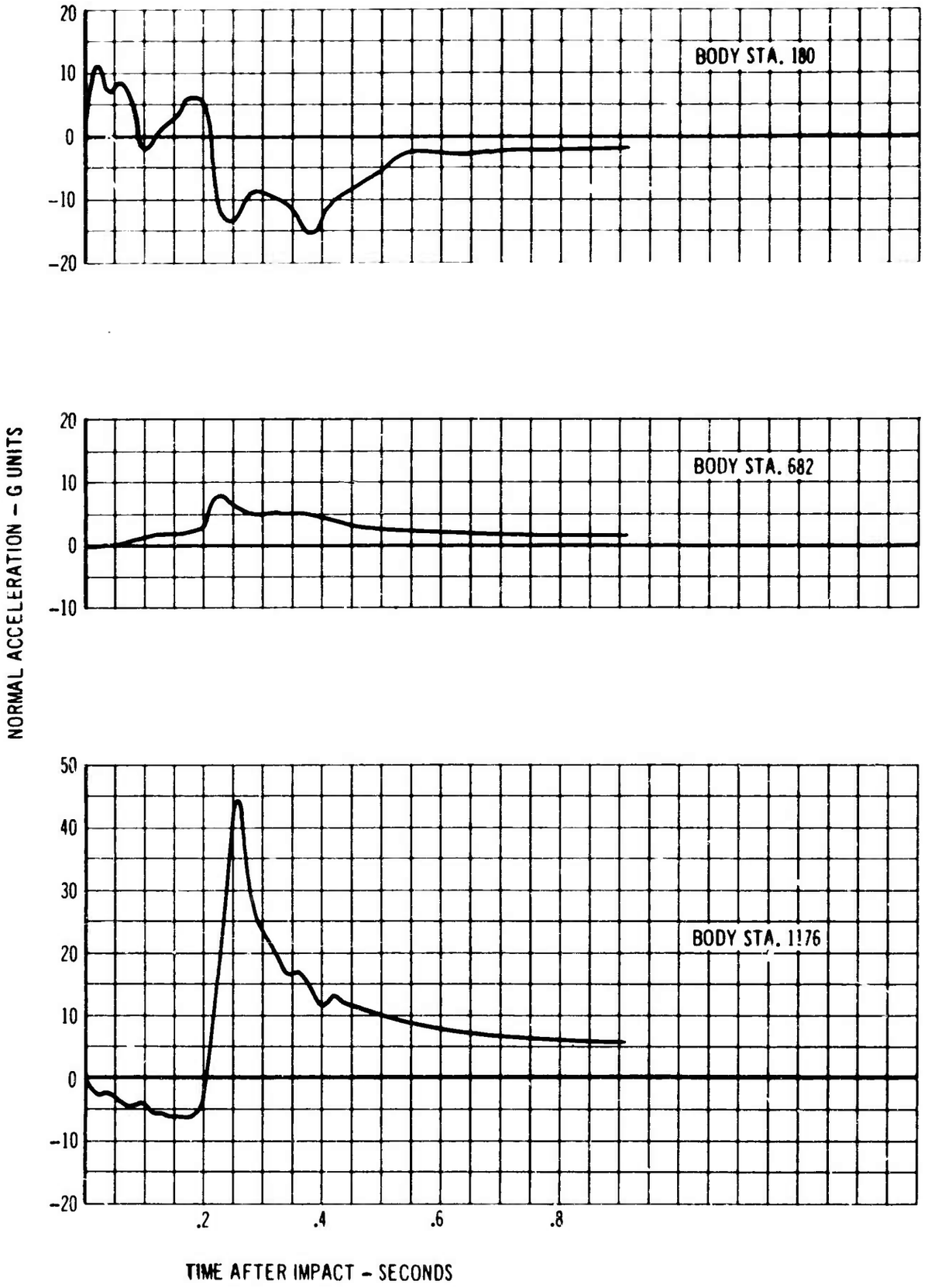

FIG. 16 ACCELERATION TIME HISTORY - FLEXIBLE BODY - 200 FT/SEC (continued)

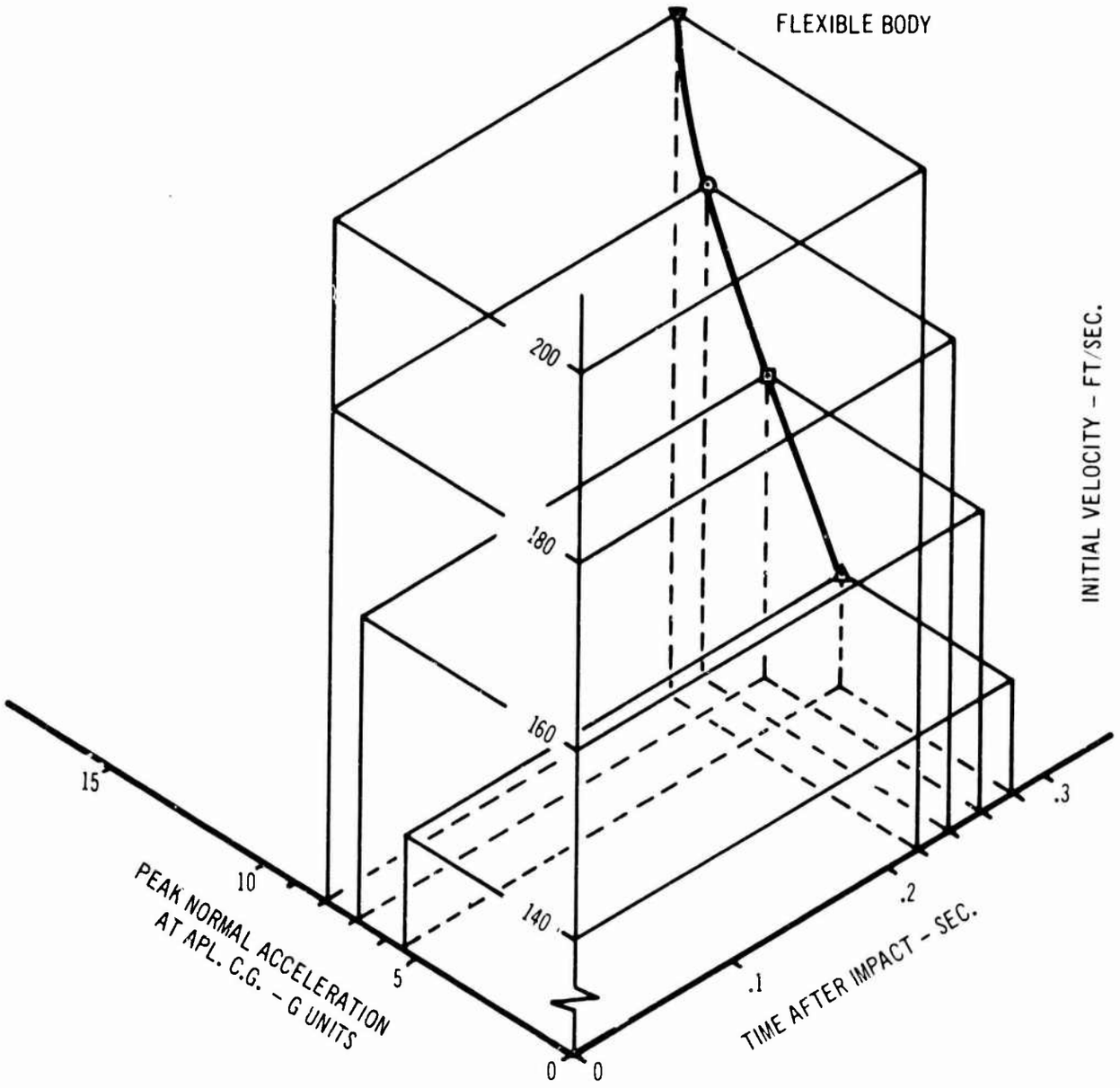

FIG. 17 ACCELERATION TIME - VELOCITY SUMMARY - FLEXIBLE BODY

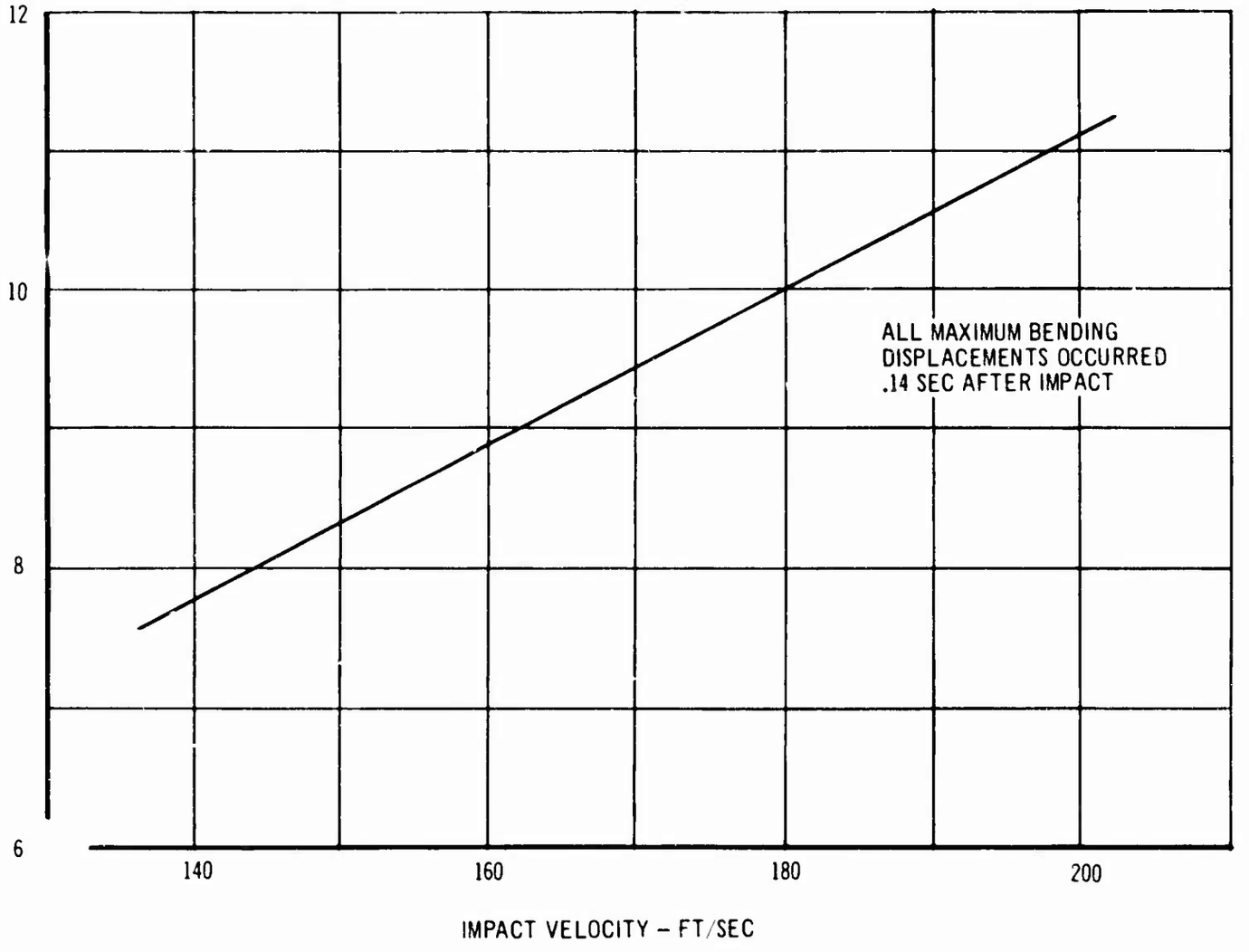

FIG. 18 MAXIMUM BENDING DEFLECTIONS AT NOSE

INITIAL CONDITIONS			
SPEED	160 FT./SEC.	C.G. LOCATION-BODY STA.	333
ANGLE OF IMPACT	6 DEGREES	PLOWING COEFFICIENT	80 LB./IN.^{2}
WEIGHT	37,800 LBS.	PLOWING AREA	432 IN.^{2}
INERTIA ABOUT C.G.	1.5×10^9 LB./IN.^{2}	FRICTION COEFFICIENT	.3

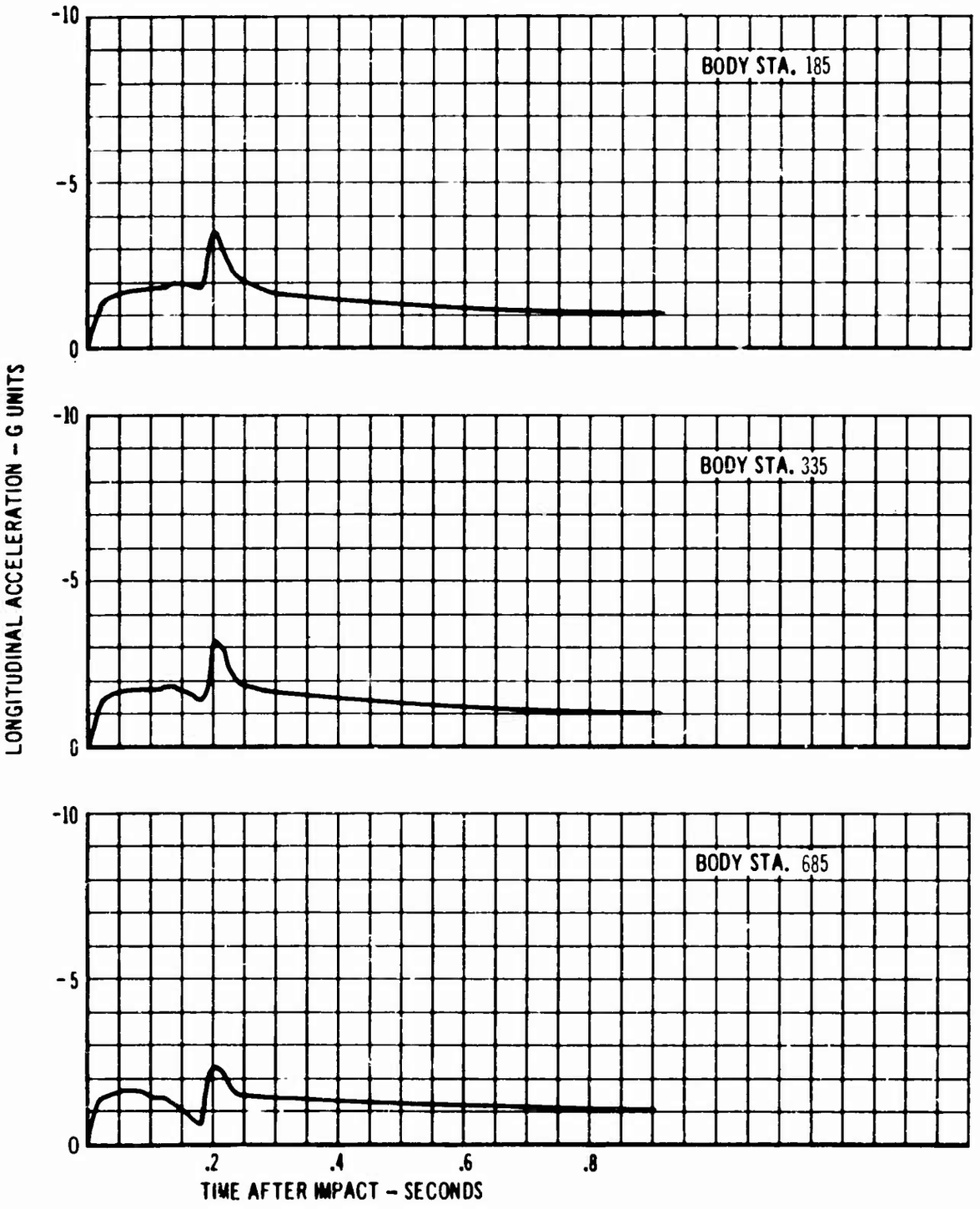

FIG. 19 ACCELERATION TIME HISTORY - CURTISS C-46

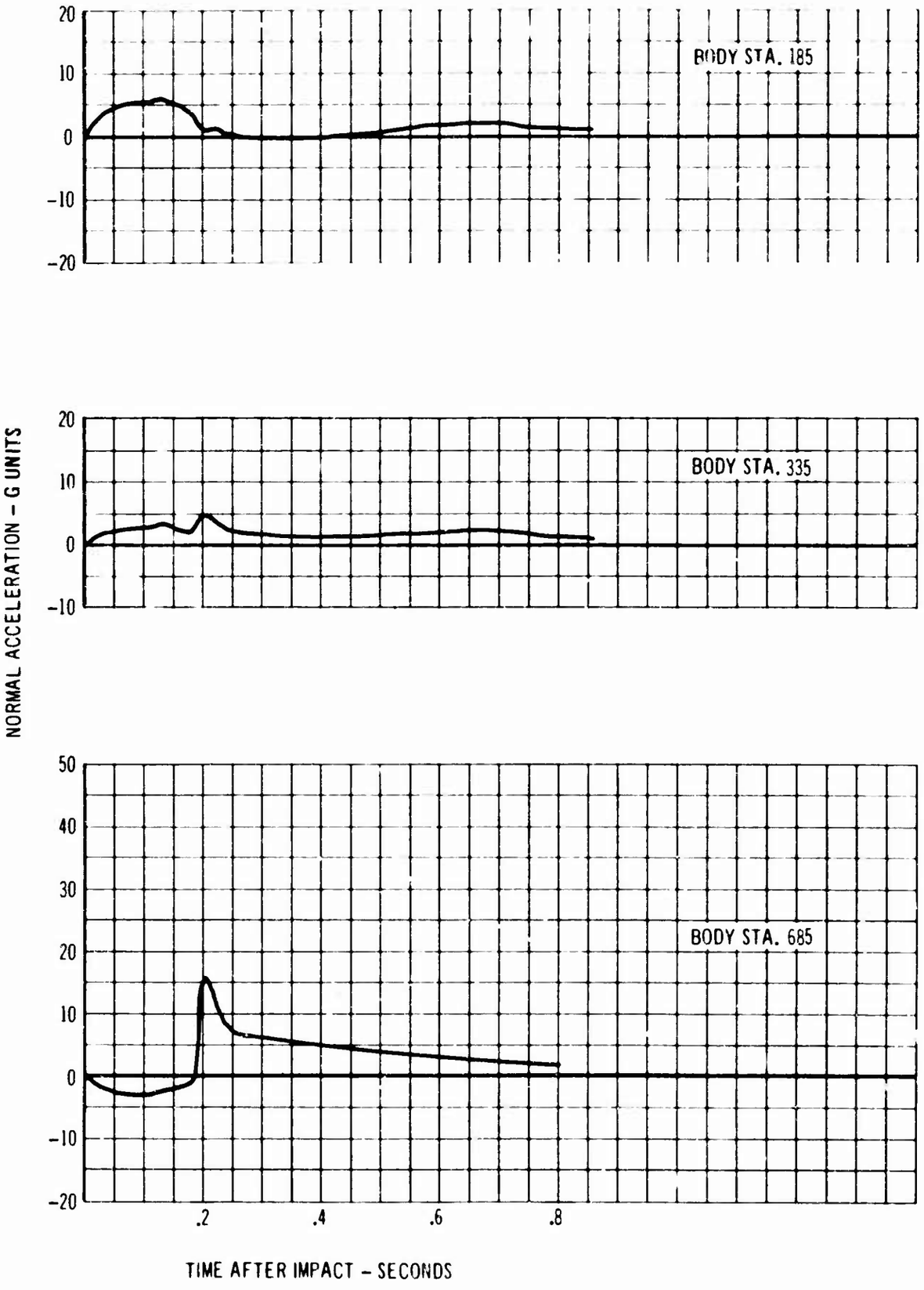

FIG. 19 ACCELERATION TIME HISTORY – CURTISS C-46 (continued)

is, a ramp angle of 6 degrees and an initial velocity of 160 feet per second. A comparison of Figs. 8 and 19 shows that in the C-46 crash, maximum accelerations and time after impact at which they occurred were somewhat less than in the Constellation crash. The general trend of the acceleration-time histories was, however, much the same.

4.3.3 Ramp Angle

Fig. 20 gives the variation with ramp angle of peak longitudinal acceleration at the airplane center of gravity and time at which it occurs. This peak is not the maximum peak G's at an approximate time after impact of 0.22 seconds, but rather is the peak caused by the initial impact force at the nose. Although results for ramp angles in excess of ten degrees are not shown, it is expected that peak values would rise sharply as the ramp angle increases. Figures 21 and 22 show the acceleration time histories for the normal and longitudinal accelerations for three ramp angle conditions.

The position of the airplane relative to the base of the ramp at impact is also important in determining peak accelerations and the time at which they occur. For example, if the airplane impacts the ramp in Position B, Fig. 21, as is the case in the Lockheed 1649 crash, the acceleration time histories will be substantially different from those in which the airplane impacts the ramp in Position A, Fig. 23. In Position A the airplane must pitch through an angle equal to that of the ramp before the understructure of the fuselage contacts the ramp's surface, whereas in Position B, only a small pitch angle is required before the tail begins to pick up load. The fuselage above the cabin floor will be more likely to fail in the impact condition of Position B since the fuselage bending moment is considerably greater.

4.3.4 Friction

The total friction force as given by Equation (8) of Section 2.1.2 is a function of the normal force on the airplane and of the friction coefficient. Maximum friction forces occur, then, at the same time as do maximum normal forces. Since peak normal forces at the airplane center of gravity may be of the order of 10 to 20 times the weight of the aircraft, the friction force is a primary quantity in the determination of peak longitudinal accelerations.

For this analysis, a nominal friction coefficient of 0.3 was assumed. This is the friction coefficient of aluminum sliding on clay as given by Ref. 9, and is believed to be close to that which will be applicable to the Lockheed crash. The friction coefficient was varied in the range of 0.3 to 0.5, and the results are shown in Fig. 24. As expected, the peak longitudinal accelerations increased with increasing friction coefficient, but the time to peak did not change.

4.3.5 Plowing Force

The plowing force is analytically determined by Equation (9) of Section 2.1.2 and is a function of the plowing coefficient and of the airplane plowing area. Both of these quantities are difficult to determine, and particularly the

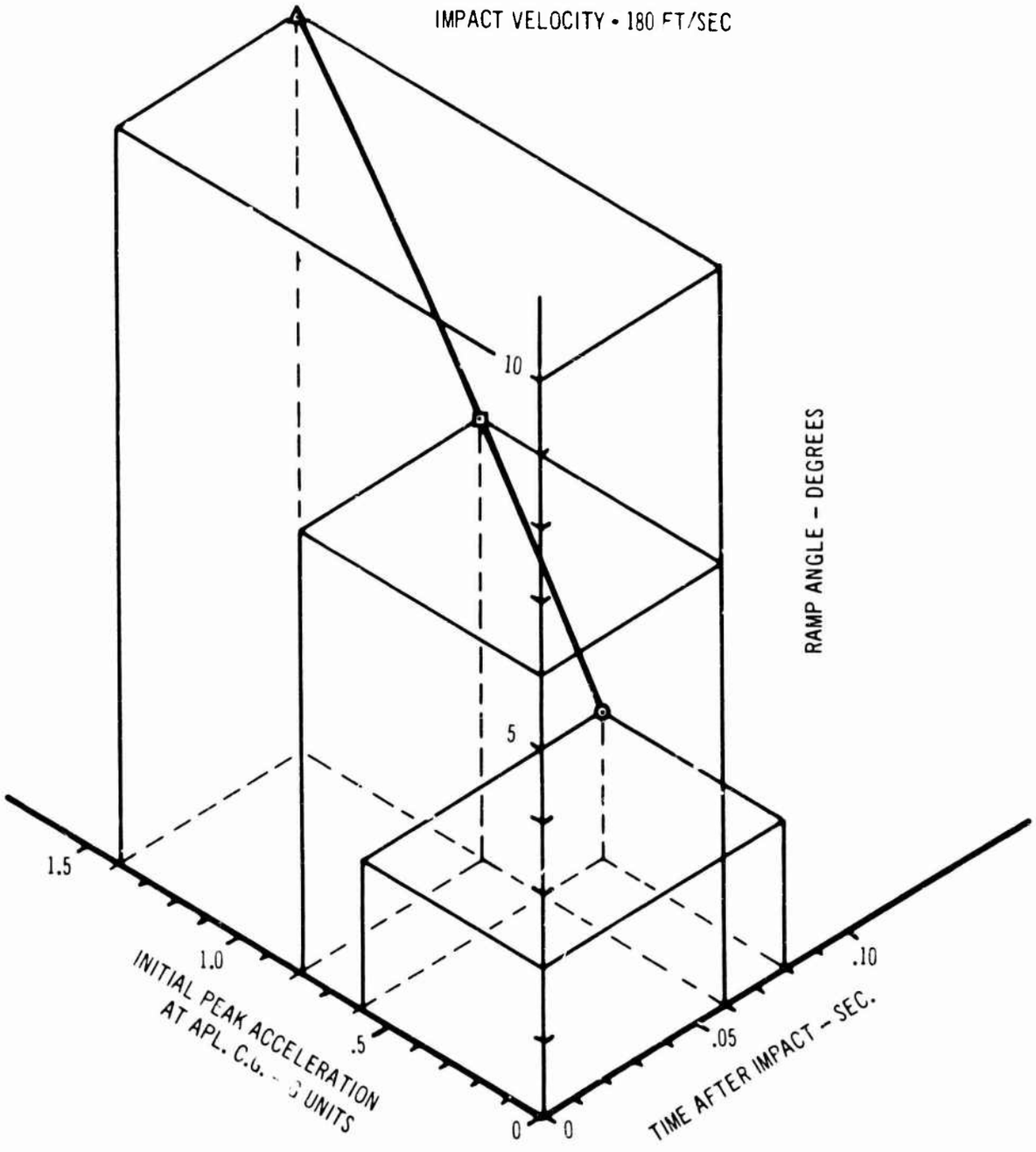

FIG. 20 EFFECT OF RAMP ANGLE ON PEAK ACCELERATIONS

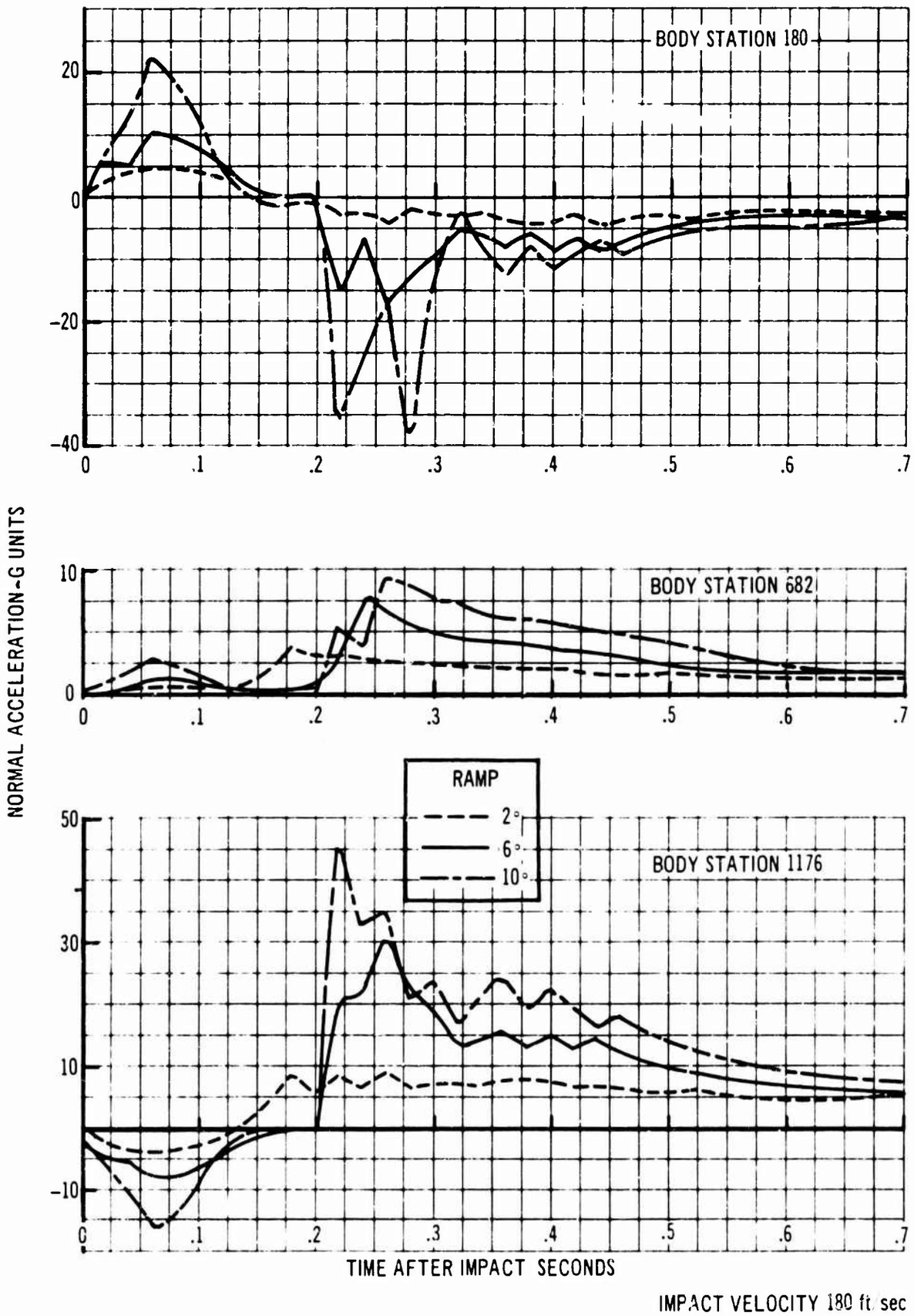

FIG. 21 RAMP ANGLE VARIATION NORMAL ACCELERATION

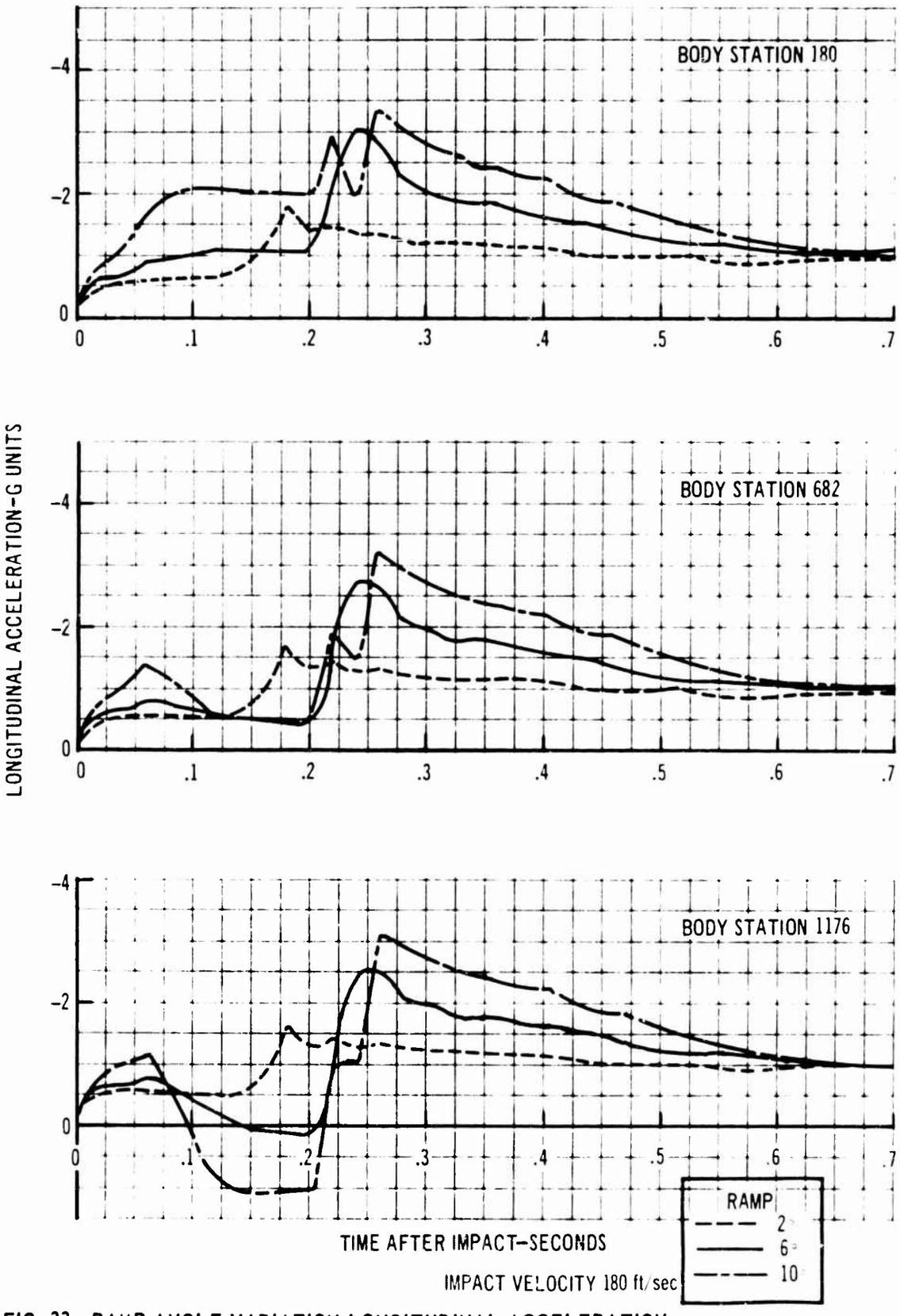

FIG. 22 RAMP ANGLE VARIATION LONGITUDINAL ACCELERATION

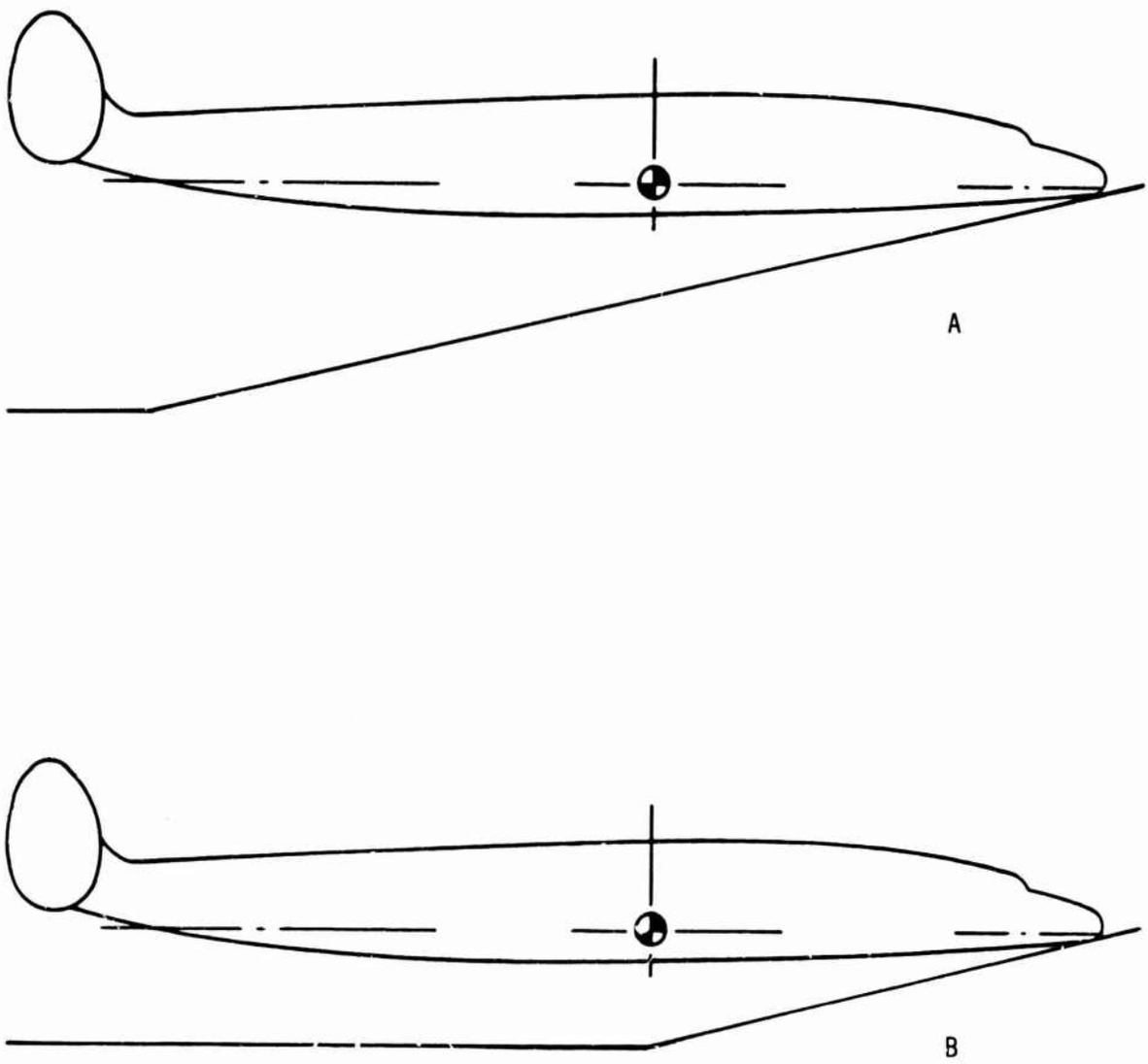

FIG. 23 POSITION OF THE AIRPLANE AT IMPACT

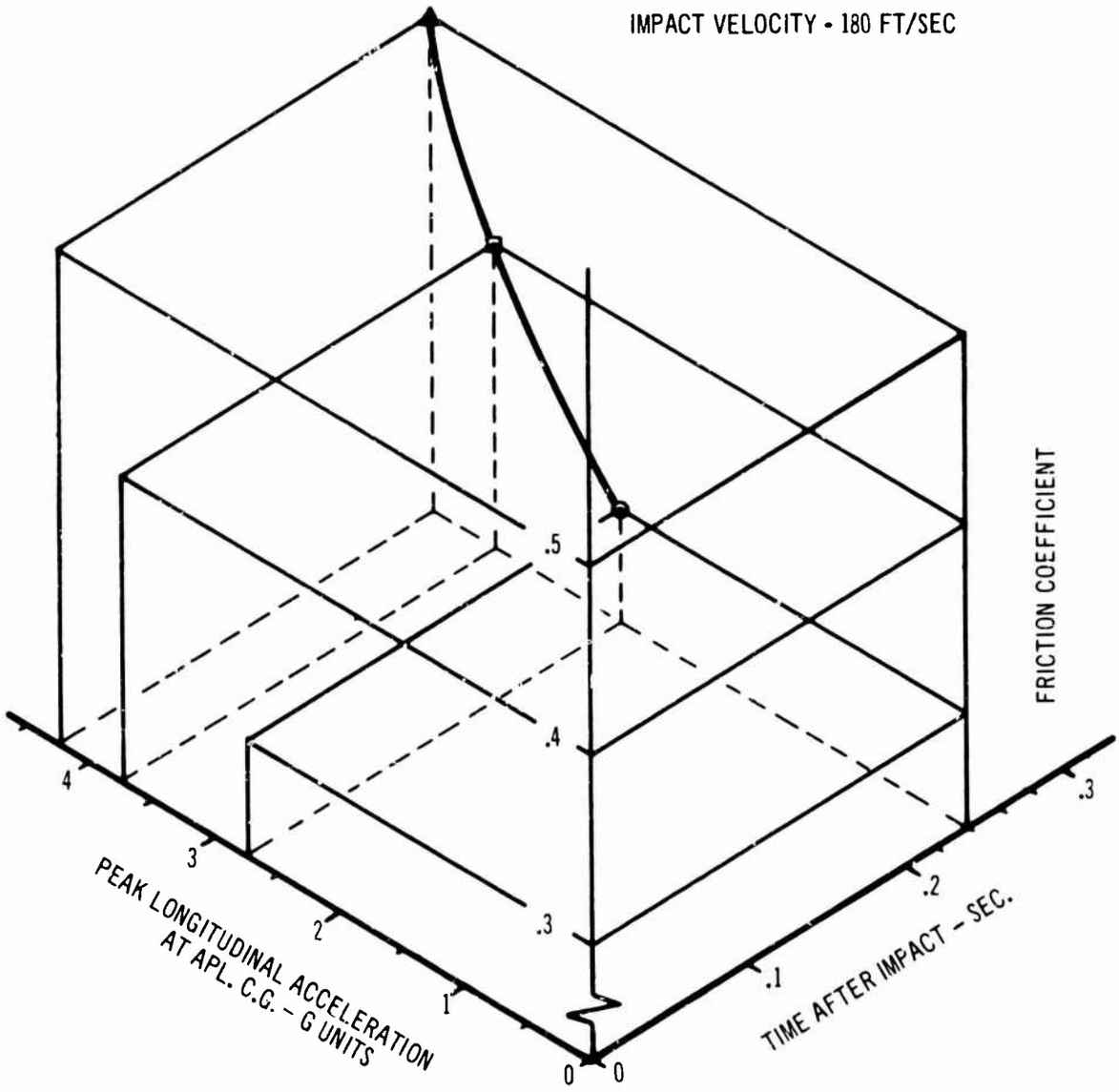

FIG. 24 EFFECT OF FRICTION COEFFICIENT ON PEAK ACCELERATIONS

latter since it is dependent primarily on the depth of penetration of the airplane into the ground. This, in turn, is a function of the weight and geometry of the airplane, the deformation characteristics of both the airplane and ground, and the angle at which the aircraft impacts. However, results have indicated that in the 1649 crash peak longitudinal accelerations, which are most affected by the plowing force in low angle of impact crashes, are determined primarily by the friction force. The effects of an increase in plowing force are illustrated in Fig. 25. Tripling the plowing coefficient increased the peak longitudinal accelerations from 2.7 G's to 3.4 G's, a substantially lower rate of increase than would be obtained by tripling the friction coefficient as indicated by Fig. 22.

No experimental data on the plowing coefficient at the crash test site was available, and a nominal value of 80 pounds per square inch of plowing area was chosen. This is similar to that used in the calculations of Ref. 9. A nominal plowing area of 700 square inches was estimated based on the data of Ref. 9 and a study of the 1649 geometry.

4.3.6 Damping Forces

Damping forces are considered to be those forces in the crash which are directly proportional to the velocity of the airplane normal and downward into the ramp. They arise primarily from the friction of deformation of the ground and understructure of the airplane. For the 1649 crash a structural damping of 0.25 was assumed.

The damping was found to have some effect on the acceleration time histories. For this reason, and since the structural damping coefficient is impossible to determine with any great amount of precision, it was varied in the range of 0.100 to 0.500. A summary plot showing peak normal accelerations at the center of gravity for each of three damping coefficients is given in Fig. 26.

In general, a decrease in damping coefficient was found to slightly increase the peak normal accelerations at 0.07 seconds after impact and decrease both the magnitude and time of the maximum peak accelerations occurring at approximately 0.24 seconds. This correspondingly reduced maximum longitudinal accelerations.

4.3.7 Ground Elasticity

Inclusion of the effective spring stiffness of the ground had little effect on the results. The ground spring was considered to act in series with the structural spring of the understructure of the fuselage as per Section 2.1.2. Experimental data from the crash test site gave a California Bearing Ratio (CBR) rating of 30-50 to the soil in the impact area. This was converted to an approximate spring stiffness of 500,000 pounds per inch which was substantially greater than that of the structural springs. For this reason, when the ground spring was placed in series with the structural spring, the stiffness of the structural spring dominated the net resultant stiffness, and the effect of the ground spring was negligible.

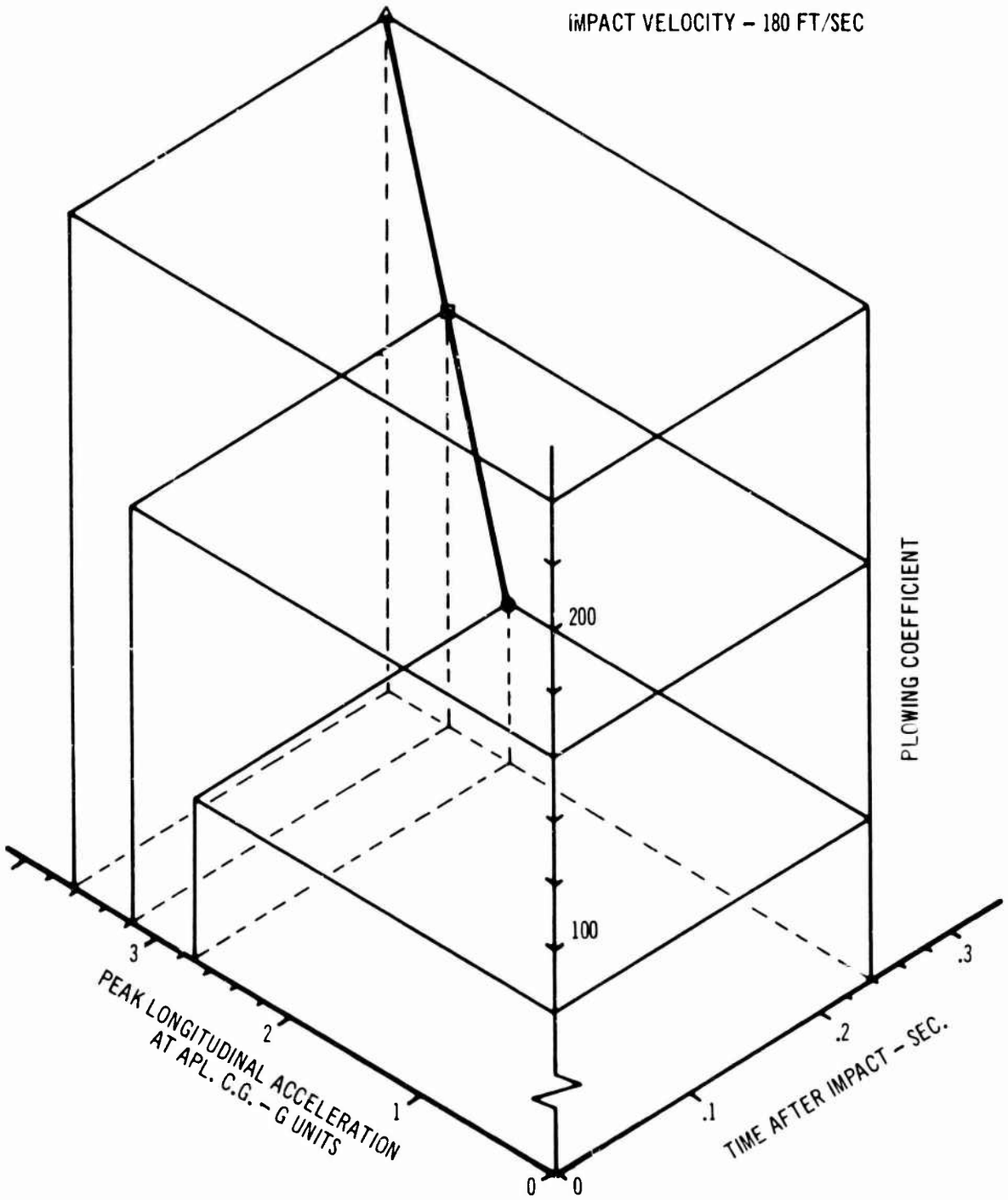

FIG. 25 EFFECT OF PLOWING COEFFICIENT ON PEAK ACCELERATIONS

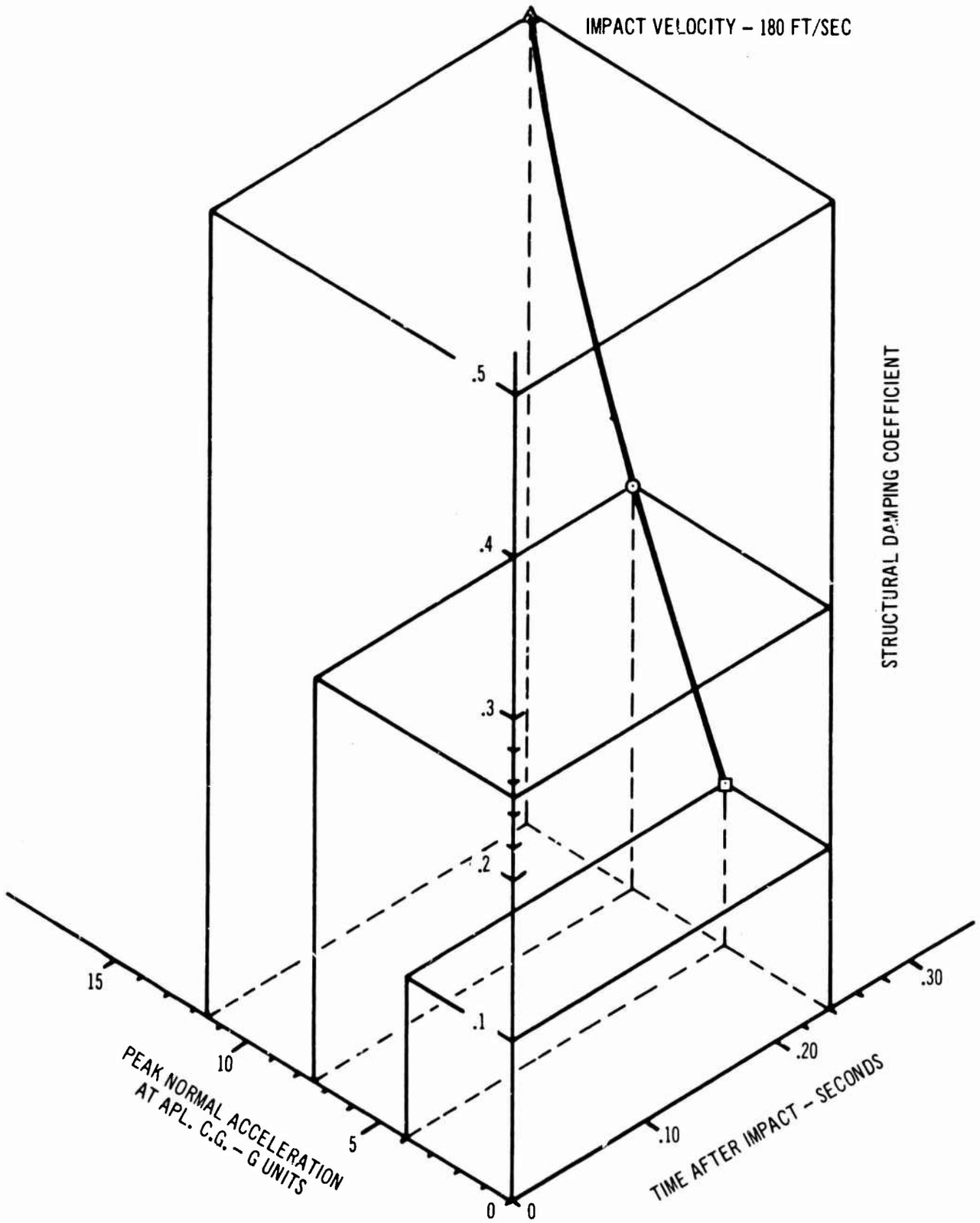

FIG. 26 EFFECT OF STRUCTURAL DAMPING COEFFICIENT ON PEAK ACCELERATIONS

5.0 CONCLUSIONS

- At initial impact of the Lockheed Model 1649 at a velocity of 180 feet per second, a force from the ground acting at the nose of the airplane will cause it to pitch up sharply.

- During this initial impact phase, peak normal accelerations of 11, 0, and -3 G's will be developed approximately 0.03 seconds after impact at Body Stations 180, 682, and 1176 respectively. At this point in time, an airplane longitudinal acceleration of 1 G's will be experienced.

- The nose of the airplane will bend upwards 10 inches relative to the center section of the fuselage at a time after impact of 0.14 seconds. This deflection will probably be of sufficient magnitude to cause the ultimate strength of the fuselage above the cabin floor to be exceeded.

- If the fuselage above the cabin floor should fail, all analytical results beyond the time of failure will be questionable to a degree dependent on the type of failure that occurs.

- If the fuselage above the cabin floor does not fail, maximum normal and longitudinal accelerations during the 6 degree ramp crash will occur at a time after impact of 0.24 seconds. Maximum normal acceleration at Body Stations 180, 682, and 1176 will be -17, 8, and 35 G's respectively. Maximum longitudinal accelerations will be 4 G's.

6.0 RECOMMENDATIONS

- Further studies are necessary to better define the effects of initial crash conditions, and airplane weight, geometry, and structural characteristics on crash loads for different aircraft.

- Improved analytical or experimental data are required for determining the crushing strength, plowing area, and structural damping of an airplane during a crash.

- The influence of airplane roll, yaw, and lateral translation on crash loads should be studied.

- If a sufficient amount of crash loads data can be obtained, it should be used to improve the accuracy of required airplane crash load factors. It should also be used to define dynamic, rather than static, test specifications for items of equipment which must function during a crash. Included in this equipment would be passenger, crew, and cargo restraints, and shock absorption systems.

7.0 REFERENCES

1. Theoretical Determination of Crash Loads for a Lockheed 1649 Aircraft in a Crash Test Program, Technical Proposal, Document D6-8603, The Boeing Company, December 1963

2. Test Plan - Full Scale Transport Crash Test Program, Contract No. FA-WA-4569, Aviation Safety Engineering and Research, November 1963

3. Liu, F., and Makky, S., On Dynamic Responses of an Aircraft During Crash Landing, Document D6-9208, The Boeing Company, February 1963

4. Synthesis of Impact Acceleration Technology for Aviation Crash Injury Prevention (Project SIAT), TRECOM Technical Report 63-31A, June 1963

5. Hoekstra, H. D., and Hoover, I. H., The FAA Aircraft Safety Development Program, Paper No. 63-44, The Institute of Aerospace Sciences, January 1963

6. United States Army Aviation Crash Injury Research, TRECOM Technical Report 63-23, December 1962

7. McCormick, W. J., Dynamic Analyzer, Document D2-20946, The Boeing Company, June 1962

8. Bingham, W. W., Crash Loads Investigation, 707-321C, Document D6-9066, The Boeing Company, June 1962

9. Preston, G. M., and Pesman, G. J., Accelerations in Transport Airplane Crashes, NACA Technical Note 4158, February 1958.

10. Weight Data for Structural Analysis, Lockheed Model 1649A, Report No. 11249, Lockheed Aircraft Corporation, February 1956

11. Gill, S., A Process for the Step-by-Step Integration of Ordinary Differential Equations in an Automatic Digital Computing Machine, Proc. Cambridge Phil. Soc., Volume 47, Pages 96-108, 1951

12. Wignot, J. E., Combs, H., and Ensrud, A. F., Analysis of Circular Shell-Supported Frames, NACA Technical Note 929, May 1944

13. Norris, C. H., et al., Structural Design for Dynamic Loads, McGraw Hill, New York, 1959

14. Bisplinghoff, R. L., et al., Aeroelasticity, Addison-Wesley, Cambridge, Massachusetts, 1955

15. Kolsky, H., Stress Waves in Solids, Oxford University Press, 1953